A MONTE CARLO STUDY OF LONG-LIVED PARTICLES (NEUTRALINOS) IN CMS AT LHC

M. Sc Thesis
in
Engineering Physics
University of Gaziantep

Supervisor
Assoc. Prof. Dr. Ayda BEDDALL
Co-supervisor: Asst. Prof. Dr. Andrew BEDDALL

By
Başak UNTUÇ
February 2009

T.C.
GAZİANTEP UNIVERSITY
GRADUATE SCHOOL OF
NATURAL AND APPLIED SCIENCES
ENGINEERING PHYSICS

Name of the Thesis	:	A Monte Carlo Study of Long-Lived Particles (Neutralinos) in CMS at LHC
Name of the Student	:	Başak UNTUÇ
Exam Date	:	02.02.2009

Approval of the Graduate School of Natural and Applied Sciences.

Prof. Dr. Ramazan KOÇ
Director

I certify that this thesis satisfies all the requirements as a thesis for the degree of Master of Science.

Prof. Dr. Ramazan KOÇ
Head of Department

This is to certify that we have read this thesis and that in our opinion it is fully adequate, in scope and quality, as a thesis for the degree of Master of Science.

Asst. Prof. Dr. Andrew BEDDALL
Co-Supervisor

Assoc. Prof. Dr. Ayda BEDDALL
Major Supervisor

Examining Committee Members:

Prof. Dr. Zihni ÖZTÜRK _____

Assoc. Prof. Dr. Ayda BEDDALL _____

Asst. Prof. Dr. Güler YILDIRIM _____

Asst. Prof. Dr. Eser OLĞAR _____

Asst. Prof. Dr. Andrew BEDDALL _____

ABSTRACT

A MONTE CARLO STUDY OF LONG-LIVED
PARTICLES (NEUTRALINOS) IN CMS AT LHC

UNTUÇ, Başak

M. Sc in Engineering Physics

Supervisor: Assoc. Prof. Dr. Ayda BEDDALL

Co-Supervisor: Asst. Prof. Dr. Andrew BEDDALL

February 2009, 62 pages

In this study after giving a summary of Standard Model (SM) which is the best theory to explain the fundamental particles and the interactions between them upto now, the Minimal Supersymmetric Standard Model (MSSM), a preferred extension of SM was given in detailed. The simulation of neutralinos which are considered to be one of the particles of structure of the dark matter and could not be explained by SM, creates the objective of this thesis. Simulations have been performed for a center of mass energy $\sqrt{s} = 10$ TeV and neutralino mass $M_0 = 165$ GeV. One hundred events have been generated using the Monte Carlo simulation method. A pair of neutralinos were produced and each of them was decayed into two jets. Two parameters have been used to investigate neutrolino signatures. One of parameters was muon decay vertex coming from decay process in four jets up to 3 cm in the inner tracker. Reconstructed muon data have been checked for all directions, then demonstrated in these directions. The other parameter was missing transverse energy coming from jets transversing Calorimeter. The related graphs have been plotted for these particles.

Key words: LHC, CMS, CMSSW, Neutralino Simulation, MSSM

ÖZET

UZUN ÖMÜRLÜ PARÇACIKLARIN (NÖTRALİNOLARIN)
LHC DEKİ CMS DE MONTE CARLO ÇALIŞMASI

UNTUÇ, Başak
Yüksek Lisans Tezi, Fiz. Müh.
Tez Yöneticisi: Doç. Dr. Ayda BEDDALL
Tez Yönetici Yardımcısı: Yrd. Doç. Andrew BEDDALL
Şubat 2009, 62 sayfa

Bu çalışmada maddenin temel yapıtaşları ve bunlar arasındaki etkileşmeleri açıklamak için şimdiye kadar ki en iyi teori olan Standart Model (SM) hakkında özet verdikten sonra, SM'in tercih edilen genellemesi olan Minimal Süpersimetrik Standart Model (MSSM) detaylı olarak verilmiştir. Standart Modelle açıklanamayan ve karanlık maddenin yapısını oluşturduğu düşünülen parçacıklardan biri olan nötralinoların simulasyonu bu çalışmanın temelini oluşturmuştur. Simulasyonlar $\sqrt{s} = 10$ TeV kütle merkezi enerjisi ve $M_0 = 165$ GeV nötralino merkez kütlesi kullanılarak yapılmıştır. Monte Carlo simulasyon yöntemi kullanılarak 100 olay üretilmiştir. Her bir olay için bir çift nötralino üretilip, buna bağlı olarak her bir nötralino iki jete bozundurulmuştur. Araştırmanın kapsamında iki parametreden yararlanılmıştır. Dahili izcinin içinde 3 cm'ye kadar oluşan muon bozunum verteksleri ve Kalorimetre'deki kayıp geçiş enerjileri parametreler olarak kullanılmıştır. İlgili grafikler çizdirilerek bölüm içerisinde sunulmuştur.

Anahtar kelimeler: LHC, CMS, CMSSW, Nötralino Simulasyonu, MSSM

I dedicate this work to my family

ACKNOWLEDGEMENTS

I would like to express profound gratitude to my advisor, Assc. Prof. Dr. Ayda Beddall, for her invaluable support, encouragement, supervision and useful suggestions throughout this research work. Her moral support and continuous guidance enabled me to complete my work successfully. And also i would like to thank to my co-superviser, Dr. Andrew Beddall, who gave the programming background and knowledge to me and pushed to button for the starting of this story and for his valuable suggestions throughout this study.

I want to thank to Prof Dr. Leandar Litov who accepted me as a member for joining his CMS research group in Sofia University. I always felt like at home in Sofia University. Also I would like to thank to Dr. Borislav Pavlov. Not only about this thesis but also his support and helps in my Sofia days. Of course all member of Sofia CMS should not be forgetten to thank.

And finally, I want to express the gratitude for my family's support in all respects during my studies and thank to E.Ulaş SAKA, who made this stressfull time even more wonderfull, for his spiritual support.

TABLE OF CONTENTS

CHAPTER

LIST OF TABLES

Table

LIST OF FIGURES

Figure

LIST OF ABBREVATIONS

AOD: Analysis Object Data

ATLAS: A Toroidal LHC Apparatus

BSM: Beyond Standard Model

C: Charge

CMS: Compact Muon Solenoid

CMSSW: CMS Software

CSC: Cathode Strip Chamber

DAQ: Data Acquisition System

DC: Drift Chamber

DE: Dark Energy

DM: Dark Matter

DT: Drift Tube

EB: Electromagnetic Calorimeter Barrel

ECAL: Electromagnetic Calorimeter

EDM: Event Data Model

EE: Electromagnetic Calorimeter Endcap

HB: Hadron Barrel

HCAL: Hadronic Calorimeter

HE: Hadron Endcap

HF: Hadron Forward

HO: Hadron Outer

HPD: Hybrid Photodiodes

IP: Impact Parameter

LEP: Large Electron Positron Collider

LHC: Large Hadron Collider

LHCB: Large Hadron Collider B-physics

MB: Muon Barrel

ME: Muon Endcap

MSSM: Minimal Supersymmetry Extension of Standard Model

P: Parity

PSET: Parameter Set

PV: Primary Vertex

RECO: Reconstructed

RPC: Resistive Plate Chamber

RPV: R-Parity Violating

SLHA: Susy Les Houches Accord

SM: Standard Model

SSB: Spontaneous Symmetry Breaking

SUSY: Supersymmetry

T: Time

TEC: Tracker Endcap

TIB: Tracker Inner Barrel

TID: Tracker Inner Discs

TOB: Tracker Outer Barrel

TOTEM: Total Cross Section, Elastic Scattering and Diffraction Dissociation

WIMP: Weakly Interacting Matter Particle

WLS: Wave Length Shifter

YB: Yoke Barrel

CHAPTER 1

INTRODUCTION

The Standard Model (SM) is a collection of three gauge theories describing particles and their interactions via force carring gauge particles. Spin is a very fundamental quantum number defining the character of particles; spin half integers (fermions) and spin integers (bosons). These gauge theories describe three fundamental forces of nature but an exception, gravitation. Meanwhile there stands SM and gravitation on different sides of physics. This the one of the main problem of physics, naturally physicists. Although there are numerous candidates to unify all forces, one of them will be under investigation by the Large Hadron Collider (LHC). It is supersymmetry (SUSY). SUSY is unique extension of the SM and unify the forces and solves some problems of the SM.

The unification is not of course only problem of physics. One of the main problems is the structure of dark matter. All known particles of SM can not construct that kind of matter in the universe. But SUSY presents weakly interacting massive particles (WIMP) in order to construct dark matter. Physics society is getting ready to test many problems of physics. The LHC has been completed in 2008. Compact Muon Solenoid (CMS) and A Toroidal Large Apparatus (ATLAS) are two major detectors of LHC. They will search for the higgs particle of the SM and SUSY. CMS is very complex and gigantic detector to make many experiments under the roof of LHC. Naturally an experiment has two extra main building blocks; hardware and software. Hardware and software units help to record and analyse the scientific and useful data generated by a detector. In that connection, there should simulate the phenomena which will be under investigation and the detector.

As we mentioned above, SUSY presents candidate particles for dark matter called WIMP. They are long-lived particles so they can travel tens of cm in the detector. Here we focused on the detection simulations of long lived particles especially the neutralino. The Neutralino is the one of long lived particles most probable candidate of WIMP. For that purpose the simulations were prepared

using CMS software (CMSSW) and pythia event generator. Then this simulation data were converted to Reconstruct event format for triggering, analysing and validation of the event.

This thesis includes several parts. The second chapter includes a short summary of the Standard Model and Beyond the Standard Model theoretical explanations. The LHC and CMS detector and its subdetectors are given with detailed in Chapter 3. The data organisation and CMSSW are explained briefly in Chapter 4. The simulation of neutralino events is shown in Chapter 5. Finally the conclusion part is added as Chapter 6.

CHAPTER 2

THEORY

2.1 The Standard Model

The Standard Model (SM) is a well defined theory that describes the elementary particles and their fundamental interactions up to now. The particles, in this theory, are classified as fermions and bosons. The fermions, matter particles, are gathered into a group of leptons and quarks as shown in Figure 2.1. The bosons are known as intermediate interaction particles which have integer spins.

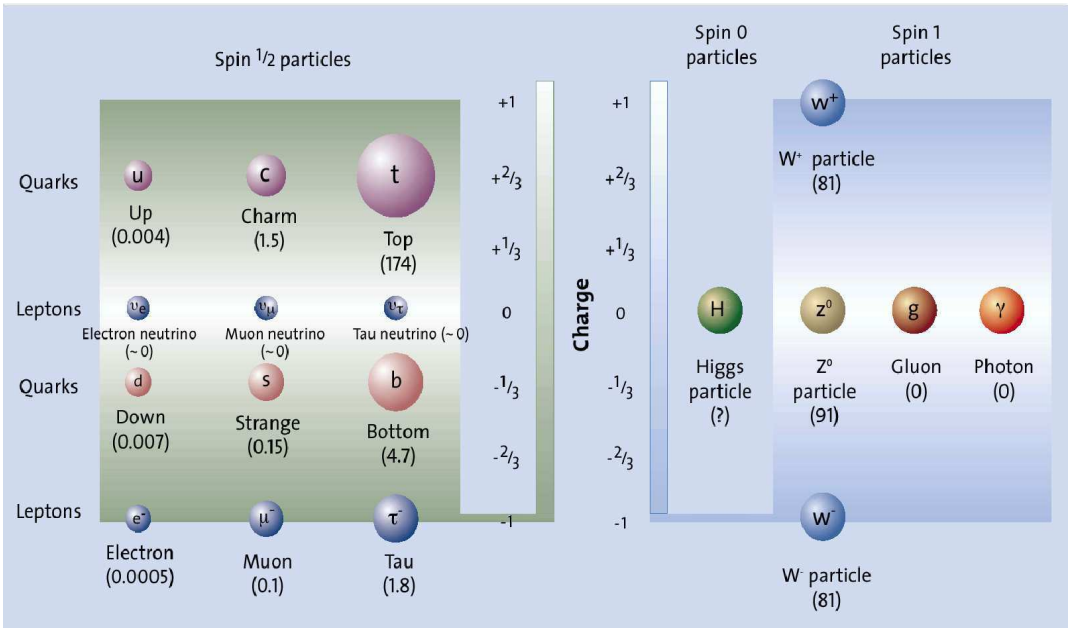

Figure 2.1: Overview of the Standard Model particles.

The model also can be defined as a quantum field theory that includes the unified weak and electromagnetic interactions (electroweak) and the strong interactions (quantum chromodynamics). Since the effects of gravity are not significant, it is not included into Standard Model yet. These four forces in the universe are shown in Table 2.1 with their relative force, strength and force carrier particles.

Table 2.1: *Fundamental forces of the Standard Model.*

Force	**Range (m)**	**Relative strength**	**Force carrier**
$ElectromagneticForce$	∞	10^{-2}	$photon$
$StrongForce$	10^{-15}	1	$gluons$
$WeakForce$	10^{-13}	10^{-2}	W, Z
$GravitationalForce$	∞	10^{-40}	$graviton$

The SM is a gauge theory, based on the group $SU(3)C \otimes SU(2)L \otimes U(1)Y$, which describes strong, weak and electromagnetic interactions, via the exchange of the corresponding spin-1 gauge fields as 8 massless gluons and one massless photon for the strong and electromagnetic interactions, respectively and 3 massive bosons, $W^{\pm}$ and Z for the weak interaction. The fermionic-matter content is given by the known leptons and quarks, which are organised in a 3-fold family structure and each quark appears in 3 different colours [1]. The electroweak quantum numbers of 3-fold family structure are shown in Table 2.2. In this table, the parameters Q, T, T_3, Y, which are called as electroweak quantum numbers, denote respectively the electromagnetic charge number, the weak isospin number, the third component of the isospin number, and the weak hypercharge number. For interactions based on gauge bosons, the electroweak quantum numbers are shown in Table 2.3 with same parameters.

Table 2.2: *The electroweak quantum numbers of Fermions.*

Family	1	2	3	Q	T	T_3	Y
Quarks	$\begin{pmatrix} u \\ d' \end{pmatrix}_L$	$\begin{pmatrix} c \\ s' \end{pmatrix}_L$	$\begin{pmatrix} t \\ b' \end{pmatrix}_L$	$2/3$ $-1/3$	$1/2$ $1/2$	$1/2$ $-1/2$	$1/3$ $1/3$
	u_R	c_R	t_R	$2/3$	0	0	$4/3$
	d'_R	s'_R	b'_R	-1/3	0	0	-2/3
Leptons	$\begin{pmatrix} \nu_e \\ e \end{pmatrix}_L$	$\begin{pmatrix} \nu_\mu \\ \mu \end{pmatrix}_L$	$\begin{pmatrix} \nu_\tau \\ \tau \end{pmatrix}_L$	0 -1	$1/2$ $1/2$	$1/2$ $-1/2$	-1 -1
	e_R	μ_R	τ_R	-1	0	0	-2

Table 2.3: *The electroweak quantum numbers of Bosons.*

Bosons (Spin 1)					
Interaction	Gauge Boson	Q	T	T_3	Y
Electromagnetic	γ	0	0	0	0
Weak	Z^0	0	1	0	0
	W	1	1	± 1	0
Strong	$g_{1...8}$	0	0	0	0

The 3 fermionic families in appear to have identical properties (gauge interactions); they only differ by their mass and their flavour quantum number. The gauge symmetry is broken by the vacuum, which triggers the Spontaneous Symmetry Breaking (SSB) of the electroweak group to the electromagnetic subgroup as shown in following form [1] :

$$(SU(3))_C \otimes (SU(2))_L \otimes (U(1))_Y \xrightarrow{SSB} (\mathrm{SU}(3))_C \otimes (U(1))_{QED}$$

The SSB mechanism generates the masses of the weak gauge bosons, and gives rise to the appearance of a physical scalar particle in the model, so-called Higgs mechanism. The SM constitutes one of the most successful achievements in modern physics. It provides a very elegant theoretical framework, which is able to describe all known experimental facts in particle physics [1].

2.1.1 Symmetries

The construction of the Standard Model is referred by relation between principles of symmetry and physics. There are various ways of classifying the different symmetries. Due to kind of parameters defining these symmetry transformations, the symmetries are categorised into two groups as discrete symmetries and continuous symmetries.

2.1.1.1 Discrete Symmetries

The parameters can take just discrete values. In Particle Physics there are several examples. Among the most relevant ones are the transformations of Parity(P), Charge Conjugation (C) and Time Reversal (T). On the other hand, by the CPT Theorem we know that all interactions must be invariant under the total transformation given by the three of them C, P and T, irrespectively of their order.

It is also known that the electromagnetic interactions and the strong interactions preserve in addition P, C and T separately, whereas the weak interactions can violate, P, C and PC [2]. The CP transformation combines charge conjugation C with parity P. Under C, particles and antiparticles are interchanged, by conjugating all internal quantum numbers, e.g., $Q \rightarrow Q$ for electromagnetic charge. Under P, the handedness of space is reversed, $x \rightarrow x$. Thus, for example, a left-handed electron e_L is transformed under CP into a right-handed positron, $(e^+)_R$. If CP were an exact symmetry, the laws of Nature would be the same for matter and for antimatter. It is observed that most phenomena are C and P-symmetric, and therefore, also CP-symmetric. In particular, these symmetries are respected by the gravitational, electromagnetic, and strong interactions. The weak interactions, on the other hand, violate C and P in the strongest possible way. In addition to parity and to continuous Lorentz transformations,there is one other spacetime operation that could be a symmetry of the interactions: time reversal T, t $\rightarrow t$ [2].

2.1.1.2 Continuous Symmetries

The parameters take continuous values. The typical examples are the rotations, generically written as $R(\theta)$, where the rotation angle θ can take continuous values. There are different kinds of continuous symmetries. Most common examples of continuous symmetry are space-time symmetries which act on the space-time like translations, rotations, and internal symmetries which act on the internal quantum numbers. Typical examples of internal symmetry are the $SU(2)$ isospin symmetry, and the $U(1)_B$ baryon symmetry.

2.1.1.3 Internal Symmetries

The internal symmetries are transformations not on the space-time coordinates but on internal coordinates, and they transform one particle to another with different internal quantum numbers but having the same mass. In contrast to the case of space-time symmetries, the irreducible representations of internal symmetries are degenerate particle multiplets. There are two distinct classes of internal symmetries. First one is global symmetries. The parameters of the transformation are independent of space-time coordinates. $SU(2)$ isospin symmetry, $SU(3)$ flavor symmetry, $U(1)_B$ baryon symmetry, $U(1)_L$ lepton symmetry can be given as example of this type of symmetry. The second member for this category is Local (Gauge) symmetries.

In local symmetries, the continuous parameters of the transformation depend on the space-time coordinates. $U(1)_{em}$ electromagnetic symmetry, $SU(2)_L$ weak isospin symmetry, $U(1)_Y$ weak hypercharge symmetry, $SU(3)_C$ colour symmetry are well defined examples for local symmetries [3] .

2.1.2 The Higgs Mechanism [3]

The assumption is made that the universe is filled with a spin-zero field, called a Higgs field, that is a doublet in the $SU(2)$ space and carries non-zero $U(1)$ hypercharge, but is a singlet in colour space. This is meant in much the same sense that space is filled with electromagnetic fields whose sources are electrically charged particles, but in the Higgs case about the sources of the Higgs field. The gauge bosons and fermions can interact with this field, and in its presence they no longer appear to have zero mass. A crucial ingredient is that states with one or more Higgs fields are not orthogonal to the ground state, like the vacuum, even though these states carry non-zero $SU(2)$ and $U(1)$ quantum numbers. That means the $SU(2)$ and $U(1)$ quantum numbers of the vacuum are non-zero, so the $SU(2)$ and $U(1)$ symmetries are effectively broken. When a symmetry is broken this way, this idea can be applied to account for the mass of gauge boson in the electroweak interaction in the Standard model. The symmetry is valid for the Lagrangian but not for the ground state of the system, it is said to be a spontaneously broken symmetry. There are a lot of questions that wait to be explained with aid of LHC experiment.

2.2 Beyond The Standard Model

Until now there is no experiment with results that are in contradiction with the predictions of the SM. But there are a lot of hints to physics beyond the SM. The SM does not explain the Dark Matter (DM) and the Dark Energy (DE), which are necessary to describe the evolution of the universe and the movements of stars and galaxies at large scales. In order to explain the whole story about our universe, more theories are needed. These theories are gathered into Beyond Standard Model (BSM). BSM is needed to solve these problems which are not found by the SM.

Some of these problems are listed as in below :

(1) **Hierarchy Problem:** This is the difference between experimental values of Higgs and its theoretically value. If the Higgs scalar field indeed has a vacuum expectation value of the right size to give the observed W and Z boson masses, $(m_H)^2$ which is one of parameters in higgs boson potential should be of the order of $(100GeV)^2$. But in SM framework, Higgs mass receives the large radiative corrections from vacuum polarisation diagrams [4]. The natural value of Higgs boson mass squared is then of the order of Λ_{UV} (Ultraviolet momentum cut off) $\approx (10)^{30}$ GeV, a factor of $(10)^{26}$ GeV higher than the experimentally determined.The difference between these two scales is known as Hierarchy problem. In order to solve this problem the new scale as $\Lambda_{UV} \ll M_{GUT}$ is needed which comes from new physics.

(2) **The flavour problem:** It is unknown why there are three generations and six flavours of leptons and quarks. According to the number of the light neutrinos as determined from the Z shape line, the existence of more than three generations is not accepted. The answer of this question can not be given in SM framework.

(3) **The size of masses:** Due to the vacuum expectation value of the Higgs masses to understand the size of masses of fermions, the size of Yukowa couplings can be evaluated. But these values are not specified by SM. In order to explain the mass-hierarchy in the lepton and quark sectors, it is needed more than SM.

(4) **Gravity:** Although the gravity force has known existence, it could not be included the $SU(3)_C \otimes SU(2)_L \otimes U(1)_Y$ gauge theory. The four fundamental forces can not be described by using the SM. This again shows that SM is not the complete theory for our universe.

(5) **Charge Quantisation:** The only understanding of the charges of all particles concern the sum of the charges of all left-handed fermions in one generation, required to be zero by anomaly cancellation [5]. The reason of charge quantisation can not be solved by SM.

(6) **Dark Matter:** The astrophysical observations such as cosmic microwave background and the structure and movement of galaxies, show that the universe contains a significant amount of the dark matter, however dark matter can not be accounted by the SM particles. Dark matter is just one of problems that are waiting to be solved by BSM.

2.2.1 Supersymmetry

The most popular extension of the SM is supersymmetry (SUSY). The SUSY is a theory which predicts a symmetry between $spin-1$ particles (bosons) and $spin1/2$ particles (fermions). SUSY is a symmetry that relates elementary particles of one spin to another particle that differs by half a unit of spin and are known as superpartners. In other words, in a supersymmetric theory, for every type of boson there exists a corresponding type of fermion, and vice-versa.

There is no direct evidence that supersymmetry is a symmetry of nature up to now. If the SUSY is the exact symmetry of nature, then particles and their superpartners (which differ in spin by half a unit) would be degenerate in mass [6]. Since superpartners have not (yet) been observed, supersymmetry must be a broken symmetry. Nevertheless, the stability of the gauge hierarchy can still be maintain if the susy breaking is soft [7, 8], and the corresponding supersymmetry-breaking mass parameters are no larger than a few TeV. So most interesting theories of this type are theories of low-energy (or $weak-scale$) supersymmetry, where effective scale of supersymmetry breaking is tied to the scale of electroweak symmetry breaking [9, 10]. A simple example of successful unification aries in the minimal supersymmetric extension of the Standard model (MSSM), where supersymmetric masses lie below a few TeV [11].

2.2.1.1 Minimal Supersymmetry [6]

The minimal supersymmetric extension of the Standard Model (MSSM) consist of taking the fields of two Higgs-doublet extension of the Standard Model and adding the corresponding supersymmetric partners [12, 13]. The corresponding field content of the MSSM and their quantum numbers are shown in Table 2.4. The electric charge $Q = T_3 + Y$ is determined in terms of the third component of the weak isospin T_3 and $U(1)$ hypercharge (Y).

The gauge super-multiplets consist of the gluons and their gluino fermionic superpartners and the $SU(2) \otimes U(1)$ gauge bosons an their gaugino fermionic superpartners. The Higgs super multiples consist of two complex doublets of Higgs fields, their higgsino fermionic superpartners and the corresponding antiparticle fields. The matter super multiplets consist of three generations of left handed and right handed quarks and lepton fields, their scalar super partners (squarks and slepton fields), and the corresponding antiparticle fields. In many supersymmetric Standard Models there is a heavy stable particle (such as neutralino) which could serve as a weakly interacting massive particles (WIMP) dark matter candidate. The existence of a supersymmetric dark matter candidate is closely tied to R-parity.

Table 2.4: *The Contents of MSSM [6].*

SuperMultiplets	Bosons	Fermionic Partners	SU(3)	SU(2)	U(1)
gluon/gluino	g	$\tilde{g}$	8	0	0
gauge	$W^{\pm}, W^0$	$\tilde{W}^{\pm}, \tilde{W}^0$	1	3	0
gaugino	B	$\tilde{B}$	1	1	0
slepton	$(\tilde{v}, \tilde{e})_L$	$(v, e)_L$	1	2	-1
lepton	$\tilde{e}_R$	e_R	1	1	-2
squark	$(\tilde{u}_L, \tilde{d}_L)$	$(u, d)_L$	3	2	1/3
quark	$\tilde{u}_R$	u_R	3	1	4/3
	$\tilde{d}_R$	d_R	3	1	-2/3
Higgs	(H_d^0, H_d^-)	$(\tilde{H}_d^0, \tilde{H}_d^-)$	1	2	-1
higgsino	(H_u^+, H_u^0)	$(\tilde{H}_u^+, \tilde{H}_u^0)$	1	2	1

- **R-Parity and Lightest Supersymmetric Particle [6]:** As a consequence of B-L (Baryon-Lepton) invariance, the MSSM possesses a multiplicative R-parity invariance, where $R = (1)^{3(BL)+2S}$ for a particle of spin S [14]. This implies that all the ordinary SM particles have even R parity, whereas the corresponding supersymmetric partners have odd R parity. The conservation of R parity in scattering and decay processes has a crucial impact on supersymmetric phenomenology. In general, these particles are highly unstable and decay into lighter states. However, R-parity invariance also implies that the lightest supersymmetric particle (LSP) is absolutely stable, and must eventually be produced at the end of a decay chain initiated by the decay of a heavy unstable supersymmetric particle.

  Consequently, the LSP in an R-parity-conserving theory is weakly interacting with ordinary matter, it behaves like a stable heavy neutrino and will escape collider detectors without being directly observed. Thus, the canonical signature for conventional R-parity-conserving supersymmetric theories is missing (transverse) energy, due to the escape of the LSP. Moreover, the LSP is a prime candidate for cold dark matter [15], an important component of the non-baryonic dark matter that is required in many models of cosmology and galaxy formation [16].

- **The Goldstino and Gravitino [6]:** In the MSSM, supersymmetry breaking is accomplished by including the most general renormalizable soft-supersymmetry-breaking terms consistent with the $SU(3) \otimes SU(2) \otimes U(1)$ gauge symmetry and R-parity invariance.

These terms parameterise our ignorance of the fundamental mechanism of supersymmetry breaking. If supersymmetry breaking occurs spontaneously, then a massless Goldstone fermion called the goldstino $\tilde{G}_{1/2}$ must exist. The goldstino would then be the LSP, and could play an important role in supersymmetric phenomenology[17]. However, the goldstino degrees of freedom are physical only in models of spontaneously-broken global supersymmetry. If supersymmetry is a local symmetry, then the theory must incorporate gravity; the resulting theory is called supergravity[18]. In models of spontaneously-broken supergravity, the goldstino is absorbed by the gravitino $\tilde{G}$ (sometimes called $\tilde{g}_{3/2}$ in the older literature), the $spin - 3/2$ superpartner of the graviton[19].

- **Split-SUSY [6]:** If supersymmetry is not connected with the origin of the electroweak scale, string theory suggests that supersymmetry still plays a significant role in Planck-scale physics. However, it may still be possible that some remnant of the superparticle spectrum survives down to the TeV-scale or below. This is the idea of split-supersymmetry [20], in which supersymmetric scalar partners of the quarks and leptons are significantly heavier than 1 TeV, whereas the fermionic partners of the gauge and Higgs bosons have masses on the order of 1 TeV or below. With the exception of a single light neutral scalar whose properties are indistinguishable from those of the Standard Model Higgs boson, all other Higgs bosons are also taken to be very heavy. The supersymmetry breaking required to produce such a scenario would destabilise the gauge hierarchy. In particular, split-supersymmetry cannot provide a natural explanation for the existence of the light Standard-Model-like Higgs boson, whose mass lies orders below the mass scale of the heavy scalars. Nevertheless, models of split-supersymmetry can account for the dark matter (which is assumed to be the LSP) and gauge coupling unification. Thus, there is some motivation for pursuing the phenomenology of such approaches [21]. One notable difference from the usual MSSM phenomenology is the existence of a long-lived gluino [22].

CHAPTER 3

DETECTOR

3.1 The Large Hadron Collider

The Large Hadron Collider (LHC), illustrated in Figure 3.1, will become the world's most energetic and largest particle accelerator with its circumference of 27 km. It is planned to start operation at the first half of 2009. The LHC is a system consisting of different accelerating machines which increase the charged particles energy stepwise until they reach the desired record value. The system is very complex and its realization is on the top of present engineering.

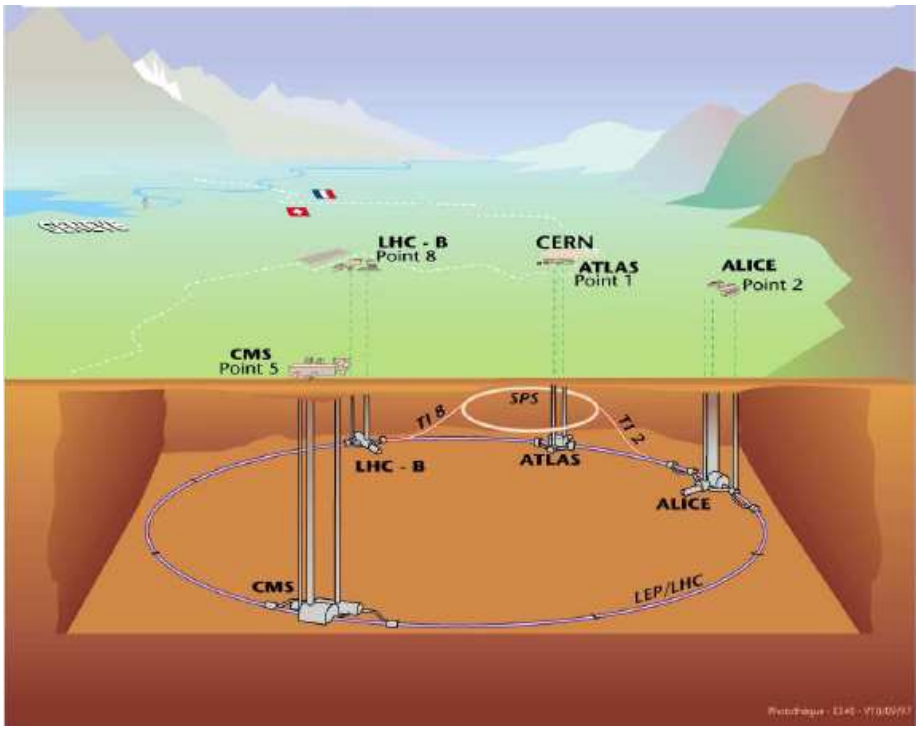

Figure 3.1: The LHC collider near Geneva, Switzerland, and the positions of the experiments along it. The pre-accelerator SPS is also shown.

The collider consists of superconducting magnets working at 1.9 K temperature with magnetic field 8.33 T. In the LHC, two particle beams are accelerated in opposite directions and made to collide in four interaction points. Physics experiments are built around these points. The A Toroidal LHC ApparatuS (ATLAS) [23] experiment is built at Point 1, just below the CERN main area, and Compact Muon Solenoid (CMS) is built at the opposite point of the collider, together with the Total Cross Section, Elastic Scattering and Diffraction Dissociation (TOTEM) experiment [24]. CMS and ATLAS experiments are general-purpose detectors designed to be able to detect various particles over a wide energy range and an almost full solid angle. Both experiments focus their effort on the discovery of the Higgs boson and therefore they both are designed to discover it over the whole range of allowed masses. Both experiments also have a large number of various other physics goals [25, 26].

Hadron colliders are suitable for verifying the predictions not only of the SM, but also of the candidates for its extensions. Machines of this type allow both TeV energies and high luminosity. This ensures detection and investigation of particles with masses on TeV scale as well as very rear processes. The experimental discovery of the spontaneous symmetry breaking (Higgs mechanism) and Higgs boson is one of the main arguments in favour of Large Hadron Collider (LHC) to be built. A center of mass energy (14 TeV) and luminosity ($L = 10^{34} cm^{-2} s^{-1}$) are chosen for proton-proton collision in such a way to ensure exploring of particle physics at TeV scale. The LHC will also be able to accelerate heavy ion beams up to energies 30 times greater than those reached by previous accelerators. This will allow observation and investigation of the properties of new matter state quark-gluon plasma. The main LHC parameters are presented in Table 3.1.

Table 3.1: *The Main LHC parameters.*

	Symbol	Each beam	pp	HI
Energy per nucleon	E	7	2.76	TeV
Dipole field at 7 TeV	B	8.33	8.33	T
Design Luminosity	L	10^{34}	10^{27}	$cm^{-2}s^{-1}$
Bunch Separation		25	100	ns
No.of Bunches	k_B	2808	592	
No.of particle per Bunch	N_p	$1.15x10^{11}$	$7.0x10^{7}$	
Collisions				
β-value at IP	β	0.55	0.5	m
RMS beam radius at IP	σ	16.7	15.9	μm
Luminosity lifetime	τ_L	15	6	hr
Number of collisions/crossing	η_c	≈ 20	-	

3.2 The CMS Detector

3.2.1 Detector Requirements

The detector requirements for CMS to meet the goals of the LHC physics programme can be summarised as follows:

- Good muon identification and momentum resolution over a wide range of momenta in the region $|\eta|< 2.5$. Good dimuon mass resolution ($\approx 1\%$ at 100 GeV/c^2) and the ability to determine unambiguously the charge of muons with 1 TeV/c (p $<$ 1 TeV/c).

- Good charged particle momentum resolution and reconstruction efficiency in the inner tracker. Efficient triggering and offline tagging of τ's and b-jets, requiring pixel detectors close to the interaction region.

- Good electromagnetic energy resolution, good diphoton and dielectron mass resolution ($\approx 1\%$ at 100 GeV/c^2), wide geometric coverage $|\eta| < 2.5$), measurement of the direction of photons and/or correct localisation of the primary interaction vertex at high luminosities.

- Good missing energy and dijet mass resolution, requiring hadron calorimeters with a large hermetic geometric coverage ($|\eta| < 5$) and with fine lateral segmentation $\triangle\eta \times \triangle\pi < 0.1 \times 0.1$.

The design of CMS described below meets these requirements .

3.2.2 The CMS Experiment

The CMS experiment [27, 28] will take place on the new built LHC. There are four experiment which are CMS, ATLAS, ALICE and LHCb on the LHC. The CMS detector is mainly composed of Magnet System, Inner Tracker, Calorimeter, Muon System and Data Acquisition System (DAQ) as shown in Figure 3.2 [29]. The detailed explanation of sub components of CMS detector is given in next pages. However as short description:

- Magnet creates 4 T magnetic field, needed for charge particles momentum measurement. The iron return yoke is used in the muon identification. Solenoidal geometry of the coil is chosen which determines the layout of the whole detector. The magnet coil is built of superconducting material operated at helium temperatures.

- Inner tracker is used for effective track and vertex reconstruction as well as for precise transverse charge particles momentum. It is based on all silicon-design pixel and microstrip detectors.

- Electromagnetic calorimeter is used for precise measurement of electron and photon energies and it is connected to trigger formation of the experiment.

- Hadronic calorimeter is used for measurement of hadrons and jet energy and connected to trigger formation of the experiment. The Hardonic calorimeter envelops the electromagnetic calorimeter and together with using for measurement of energy and direction of the hadronic jets as well as ensures the hermetisity needed for transversal missing energy.

- Muon system is utilised for identification and momentum measurement of muons and contributes to the trigger formation. The muons are characteristic of most of the interesting physical processes that will be examined at the LHC.

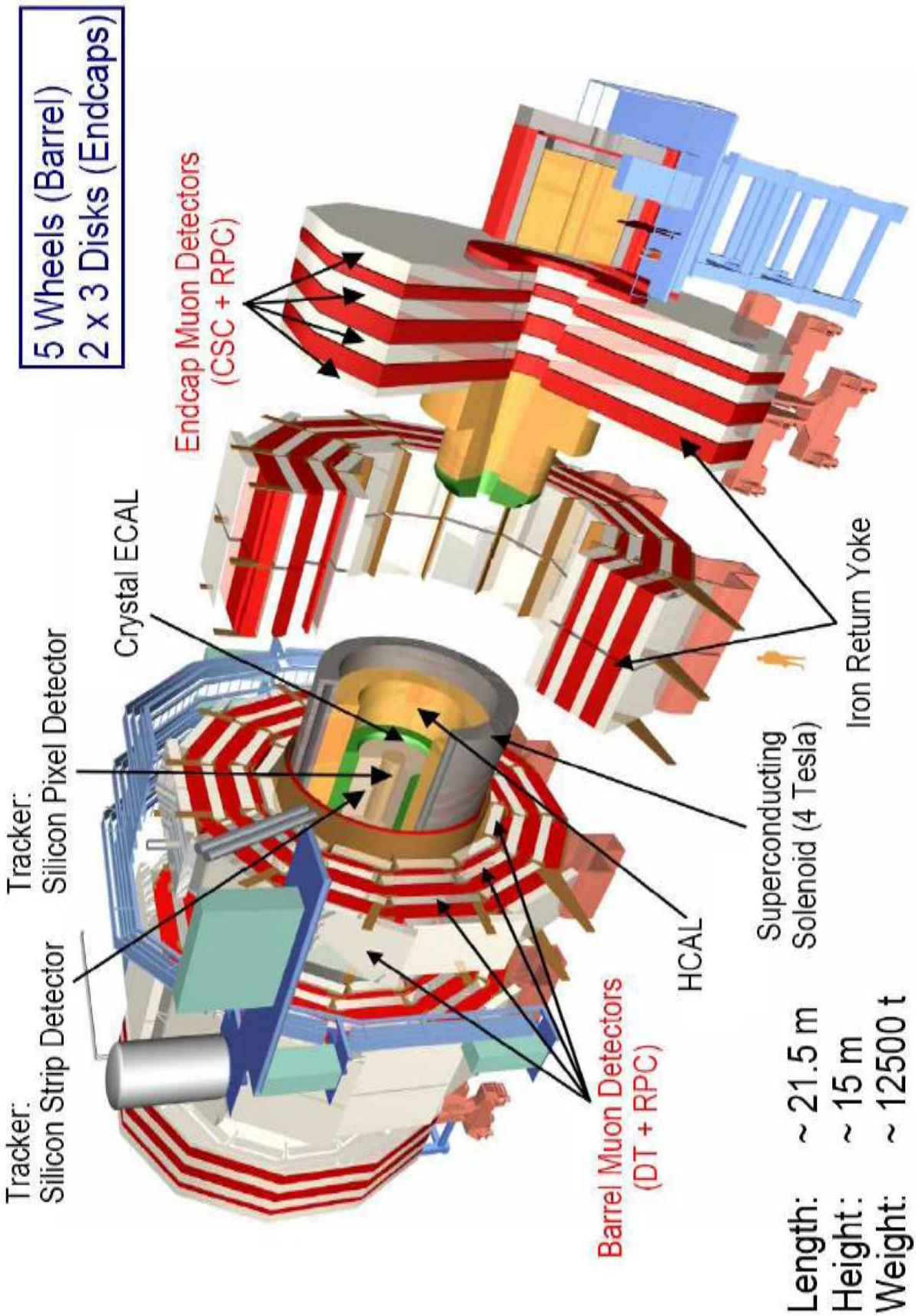

Figure 3.2: The CMS Detector.

3.2.2.1 The Magnet System

The CMS Detector has a superconducting solenoid magnet system with magnetic field of 4 T which allows a high resolution measurement of the transverse momentum of charged particles [30]. CMS chose a large superconducting solenoid with a 12.9 m long superconducting coil with an inner bore of 5.9 m that is located inside the barrel wheels [31]. In order to keep magnet superconducting it is cooled with liquid helium and fully operational desired to store energy of 2.7 GJ [30]. The magnetic field in the barrel is quite homogeneous however it has inhomogeneous field in the endcaps as shown in Figure 3.3 [32].

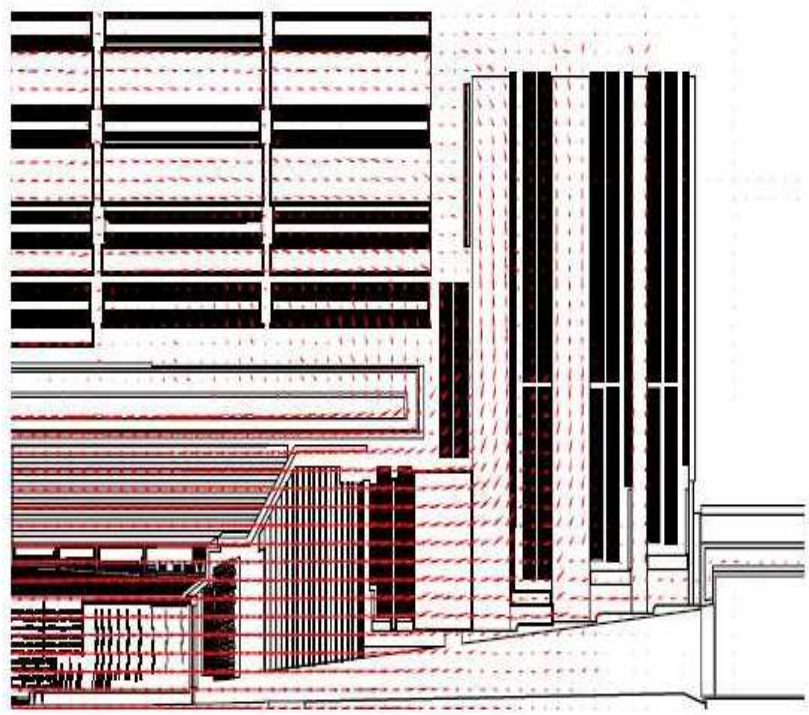

Figure 3.3: The map of CMS magnetic field.

Inside the magnet coil the electromagnetic and hadronic calorimeter as well as the main tracker are placed. This has the advantage that the calorimeter performance is not affected by the coil and a high intrinsic resolution is guaranteed.The strong magnetic field reduces the arrival of soft charged hadrons and other low energetic particles in the calorimeter and guarantees a highly performant electromagnetic calorimeter. The magnetic flux returns through the iron yoke that is instrumented with the muon system. The magnetic induction should be about 4 T in the coil and in the innermost section of end cap yoke and about 1.7 T in the barrel part of return yoke and in the outermost disk of endcap yoke.

3.2.2.2 The Inner Tracker System

The Inner Tracker System is the closest part to the beam pipe region of the CMS detector. It is desired to be able to measure the multiplicity of particles which are occurred during the pp - collision with high momentum resolution. For track reconstruction and momentum measurement close to the interaction point, the system is made by all-silicon tracker system [33] which consists of 9.6 million silicon microstrips and 66 million pixel elements [34] as shown in Figure 3.4.

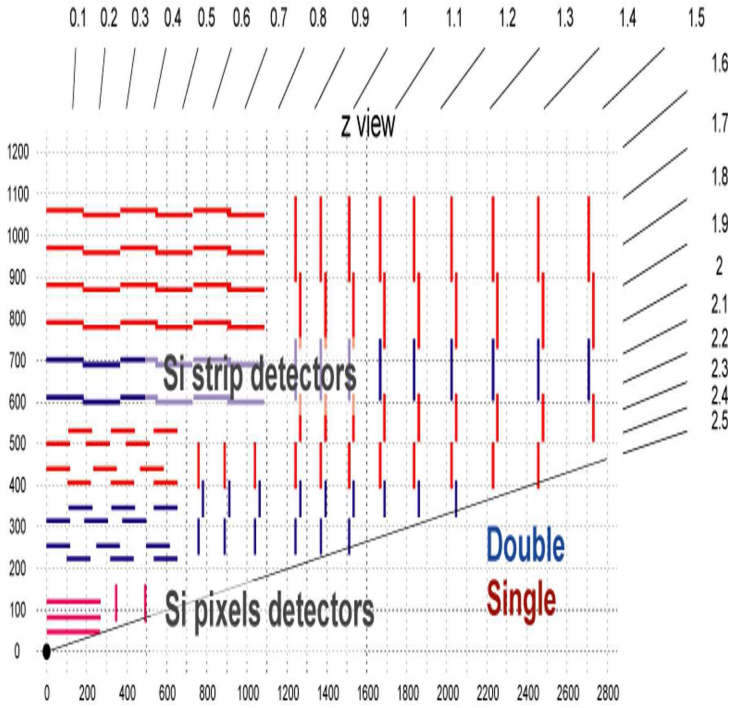

Figure 3.4: Cross section of one quarter of the CMS tracking system.

The main goal of the inner tracker is to measure coordinates of hits where a particle has passed through a detector element to identify leptons and photons for isolated electromagnetic clusters, and to measure the momentum of energetic leptons for tagging and reconstructing of b-jets and b-hadrons in these jets as well as isolated leptons and also performing a precise measurement of muon momentum together with the outer muon system [35]. The existence of tracker material gives rise for conversioning of photons to electron-positron pairs, which leads, in particular and lossing of sensitivity in the Higgs channel. Tracker material also gives rise to multiple scattering, which significantly degrades momentum resolution. The inner Tracker of CMS is divided into two parts as pixel detector and silicon strip detector which are shown in Figure 3.5 and explained in detail.

(1) **Pixel Detector** The innermost part is the pixel detector, which consists of the three barrel layers and of pixel endcap discs on each side as shown in Figure 3.6. The pixel detector is composed of two-dimensional arrays of pixel cells which are surrounded by the outer part of tracker in which silicon strip detectors. The strip detectors are composed of the Tracker Inner Barrel (TIB) and Tracker Outer Barrel (TOB), and of the two disc-like structures as Tracker Inner Discs (TID) and Tracker Endcap (TEC) as shown in Figure 3.5.

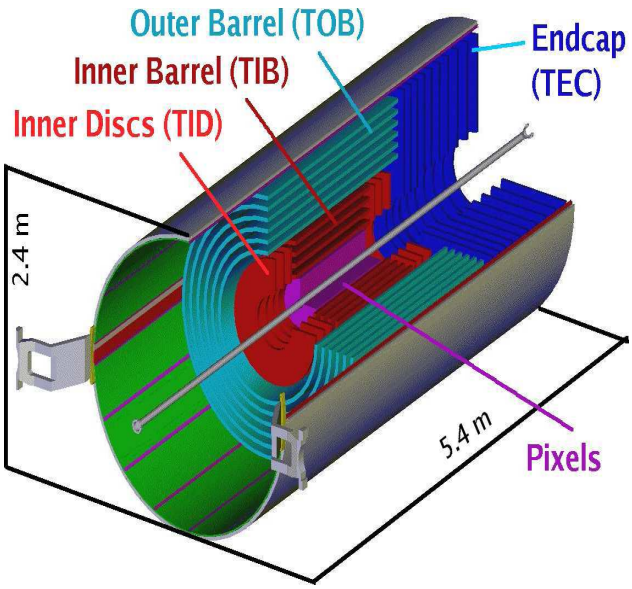

Figure 3.5: Illustration of the CMS tracker. Total weight of the tracker is about 3000 kg, including the thermal shield and support tube.

The three barrel layers are located at a mean radii of 4.4 cm, 7.3 cm and 10.2 cm, and have a length of 53 cm. The endcap discs consist of 672 pixel modules with seven different modules in each blade [36]. The endcap discs are ranged from 6 to 15 cm in radius and placed at distances of 34.5 cm and 46.5 cm from the beam line [31]. The pixel barrel layers are equipped with 768 pixel modules, which have a pixel size of 100 μm x 150 μm. Modules are arranged into half-ladders of four identical modules each. As a final choice, The sensor design which is on n-type sensor using the p-type stop isolation technique is required to meet the LHC running environments.

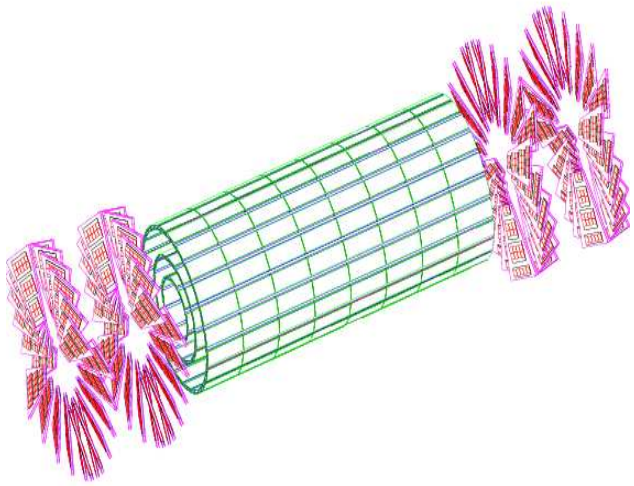

Figure 3.6: Layout of pixel detectors in the CMS tracker.

When a charged particle passes through the material, it gives enough energy for electrons to be ejected from the silicon atoms, creating electron-hole pairs. In order to pick these charges up on the surface as a small electric signal, each pixel uses an electric current produced into an electronic silicon chip which one for each tile is attached and amplified the signal [37].

(2) **Silicon Strip Detector** The silicon strip detector covers a cylindrical volume with a length of about 5.4 m and radius between 0.2 m and 1.2 m.and with an 2.1 m^2 active area which is divided into ten barrel layers and nine discs in each outer endcaps with three mini - discs arranged as in Figure 3.6. The barrel part is formed from the four-layer TIB and the six-layer TOB as shown in Figure 3.7. The two first layers in the TIB and the TOB use double-sided stereo modules consisting as in Figure 3.7. Four pixel endcap discs surround the barrel part, which consists of three layers. Length of the device is about 1 m and diameter about 30 cm. These modules provide measurements in two dimensions. The strip pitch varies in the TIB from 80 m to 120 m, and in the TOB from 120 m to 180 m.

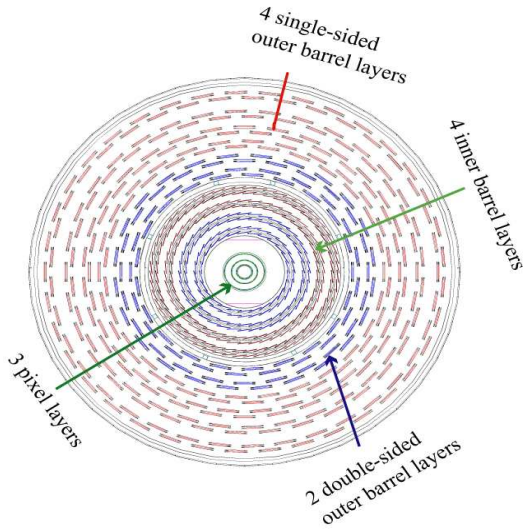

Figure 3.7: Transversal view of CMS Silicon Strip Tracker.

The endcap strip detector is made of three inner discs (TID) and nine outer discs (TEC). Modules in the concentric rings 1, 2 and 5 (counted from the beam) are double sided.

Silicon sensors are highly suited to receive many particles in a small space due to their fast response and good spatial resolution. With same working principle as in pixel detectors, as a charged particle crosses the material it knocks electron from atoms and within the applied electric field these move giving a very small pulse of current lasting a few nanoseconds. This small amount of charge is then amplified by giving as hits to reconstruct its path.

3.2.2.3 The Calorimeter

The calorimeters are used in the detector to measure the energy of the incoming particles by absorbing them. The CMS Detector has two main calorimeter as Electromagnetic Calorimeter (ECAL) and Hadronic Calorimeter (HCAL). The inner part is the ECAL which is used to measure the energies of electrons, positrons and photons. The HCAL is used to measure the energies of hadrons which deposit most of their energy within this calorimeter.

(1) **The Electromagnetic Calorimeter**

The ECAL [38] is an inorganic scintillating crystal calorimeter which is made of $PbWO_4$ crystals mounted in the central barrel part, closed by 7324 crystals in each of the 2 endcaps as shown in Figure 3.8.

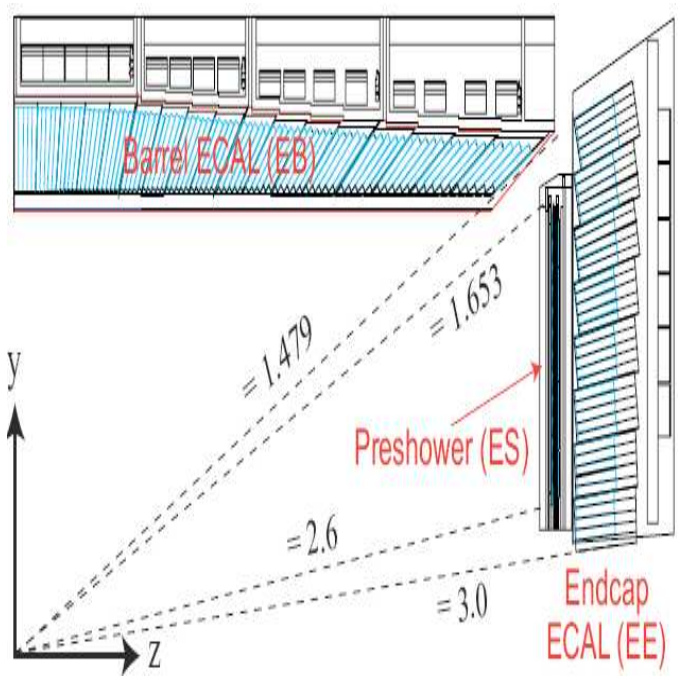

Figure 3.8: Transverse section through the ECAL, showing geometrical configuration.

In the barrel region (EB) of ECAL, which has an inner radius of 129 cm, is set as 36 identical supermodules, each covering half the barrel length and corresponding to a pseudorapidity range of $0 < |\eta| < 1.479$ [31]. The EB region has 61200 crystal modules with a dimensions of $22 \times 22 \times 230\ mm^3$. The endcaps (EE) of the ECAL, is placed at a distance of 314 cm from the vertex and covering a pseudorapidity range of $1.479 < |\eta| < 3.0$, are each set as 2 Dees, consisting of semi-circular aluminium plates from which are known as supercrystals. By having special characteristics, Lead tungstate, is used in crystals because of its high density ($8.3\ g/mm^3$), leading to a short radiation length (0.89 cm), a small Moliere radius of 22 mm and a fast scintillation time of 25 ns [31].

The energy resolution, measured by fitting a Gaussian function to the reconstructed energy distributions, can be parameterised as a function of energy in the below equation,

$$\frac{\delta(E)}{E} = \frac{S}{\sqrt{E/GeV}} \oplus \frac{N}{E/GeV} \oplus C \tag{3.1}$$

where S is the statistical term, N the noise and C the constant term [31]. The measured energy resolution $\delta(E)/E$ is 1.4 % at 10 GeV and 0.4 % at 250 GeV.

(2) **The Hadronic Calorimeter (HCAL)**

HCAL is used for measurement of hadrons and jet energy and is connected to trigger formation of the experiment. The hadronic calorimeter has a sampling structure and consists of brass plates (absorber) with thickness of 5 cm in barrel and 8 cm in the endcaps. As an active element between the plates there is plastic scintillator with thickness of 3.7 mm [31]. The light emitted from the scintillator is passed through wave length shifter (WLS) and is taken to the outer side of the calorimeter via with optic fibers where it is measured with hybrid photodiodes (HPD). The scintillators are divided into segments with size of $\triangle\eta \times\triangle\phi = 0.087\times0.087$, which provides good enough resolution to detect dijet events. This is so called "tail catcher" which is used to improve the jet absorption in the barrel outside of the magnet and its cryogenic system. In order to improve the jets measurement efficiency the absorber and the scintillator layers form projective geometry structures are oriented towards the interaction point.

The HCAL is divided into four kinds as hadron endcap (HE), hadron barrel (HB), hadron outer (HO), hadron forwad (HF) as shown in Figure 3.9. The HCAL [38, 39] is a sampling calorimeter with 50 mm thick copper absorbers interleaved with 4 mm active scintillator sheets.

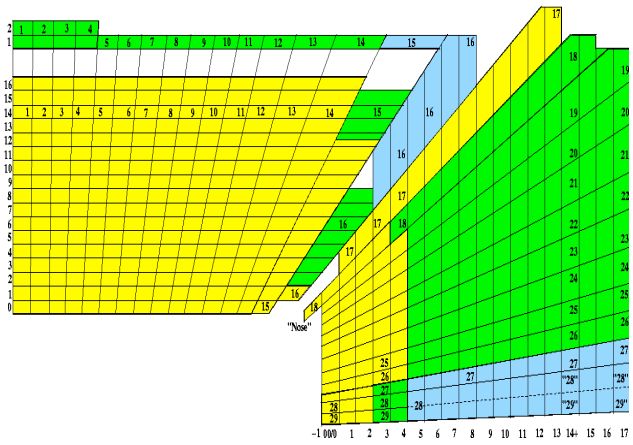

Figure 3.9: A schematic view of the tower mapping in r-z of the HCAL barrel and endcap regions.

(a) **Hadron Barrel :** The barrel hadronic calorimeter (HB) is constructed out of two 4.3 m long half-barrels [40], surrounding the tracker and the ECAL, are placed inside the magnet coil. The HB part of HCAL consists of 32 towers covering the pseudorapidity region -1.4 $<|\eta|<$ 1.4, resulting in 2304 towers with a segmentation $\triangle\eta\times\triangle\phi = 0.087 \times 0.087$. The HB is read out as a single longitudinal sampling. There are 15 brass plates, each with a thickness of about 5 cm, with 2 external stainless steel plates for mechanical strength. Particles leaving the ECAL volume first see a scintillator plate with a thickness of 9 mm rather than 3.7 mm for the other plates. The light collected by the first layer is optimised to be a factor of about 1.5 higher than the other scintillator plates.

(b) **Hadron Outer :** The outer hadronic calorimeter (HO) detector contains scintillators with a thickness of 10 mm, which line the outside of the outer vacuum tank of the coil and cover the region -1.26 $<|\eta|<$ 1.26. They sample the energy from penetrating hadron showers leaking through the rear of the calorimeters and so serve as a tail-catcher after the magnet coil. They increase the effective thickness of the hadron calorimetry to over 10 interaction lengths, thus reducing the tails in the energy resolution function. The HO also improves the E_{Tmiss} resolution of the calorimeter.

(c) **Hadron Endcap :** The endcap hadronic calorimeters (HE) are placed at each end of the barrel, so that a hermetic coverage of up to $|\eta|= 3$ is guaranteed. The end caps have about 10 nuclear interaction lengths, as the barrel calorimeter has roughly 6 interaction lengths. Extra scintillators are placed outside the magnet coil, using the solenoid as additional absorber so that a total of 11 nuclear interaction lengths in the barrel region is reached. The total number of HE towers is 2304 [40].

(d) **Hadron Forward :** The forward hadronic calorimeters (HF) cover the region $3.0 <|\eta|< 5.0$, two hadronic forward calorimeters are placed at the ends of CMS at a distance of 12 m from the interaction point. It enhances the detector hermeticity and helps for tagging of events with vector boson decays and improves the missing energy measurement as well as the acceptance of forward jets. It is built of quartz fibers situated into an iron absorber. The particles passing through the quartz emit Cherenkov radiation which is registered at the end of fibers.

3.2.2.4 The Muon System

The detection of muons with high efficiency requires a large interval of pseudorapidity $|\eta|$. For this reason the barrel part covers the region $|\eta|< 1.3$, and the endcaps $-0.9<|\eta|< 2.4$. The muon system is built of three types of detectors as drift tubes (in the barrel part), cathode strip chambers (in the endcaps) and resistive plate chambers (both in barrel and endcaps) as shown in Figure 3.10. Drift tubes and cathode strip chambers are used for precise measurement of muon tracks (and thus the momentum of muons). Resistive plate chambers are very fast and participate in the formation of the trigger of the detector. There are four cylindrical layers of drift tubes and resistive plate chambers in the barrel part and four disk-shaped layers of cathode strip chambers and resistive plate chambers in the endcaps, as the fourth layer is outside the return yoke. The magnet with its strong magnetic field and iron yoke (which at the same time is used as an absorber providing muon identification), helps these tasks.

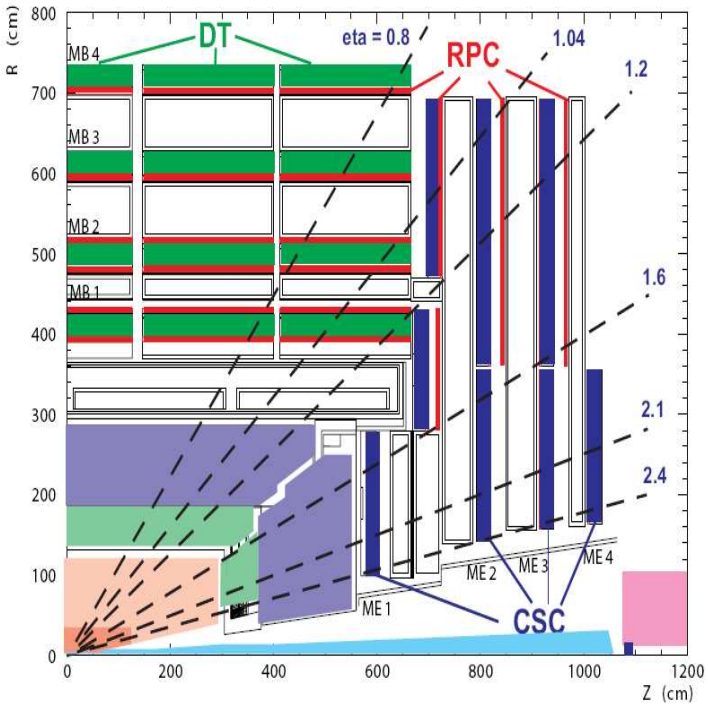

Figure 3.10: Longitudinal view of one quarter of CMS Muon Chamber.

- **Drift Tube Chamber :** The barrel region of the muon chamber is consist of drift tube chambers (DCs) and return yokes barrels (YBs). The four DCs barrels are mounted between the five yoke wheels (YB-2, YB-1, YB0, YB+1, YB+2). There are totally 250 chambers in the 4 concentric cylinder stations (MB1, MB2, MB3, MB4 from inside to outside) around the beam line. The radius of the stations changes as 4.0 m, 4.9 m,5.9 m and 7.0 m from the beam axis [31]. Each DT chamber in the 3 innermost stations, MB1-MB3, consists of 12 aluminium layers of drift tubes divided into 3 groups of 4 consecutive layers, called SuperLayers (SL) shown in Figure 3.11. Depending on the stations, In the MB1 and MB2 regions, DT chamber is placed like a sandwiched between 2 RPCs, however in the MB3 and MB4 regions, each of one DT chamber includes one RPC, which is placed on the innermost side of the station. With the aid of this design, having 6 RPCs and 4 DT chambers in the barrel region, when an high-p_T muon pass through, since the muon-track candidate can be easily built because of producing up to 44 measured points in the DT system.

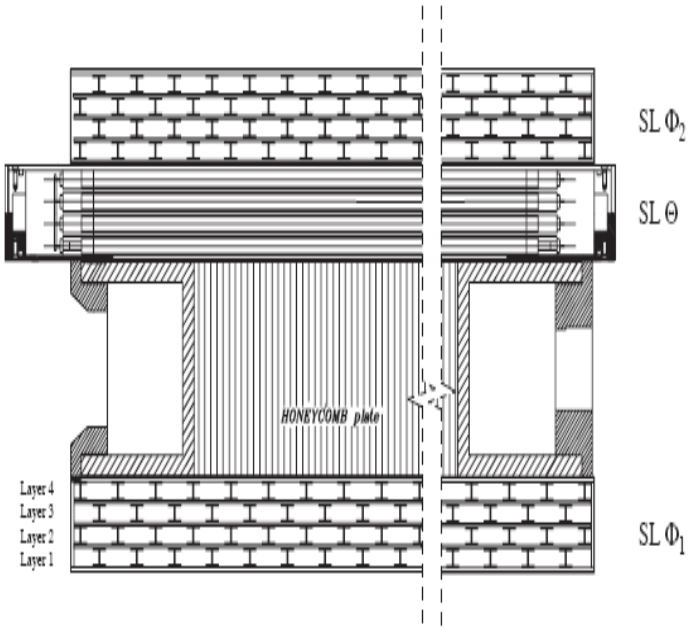

Figure 3.11: The layout of a DT chamber inside a muon barrel station.

As shown in Figure 3.11, Each DT chamber has a honeycomb structure which separates the $SL\theta$ from the other 2 $SL\phi$ s that measures the r-ϕ coordinate in the bending plane, as the $SL\theta$ measures the z-coordinate running parallel to the beam. By being a main detection elements of The Drift Tube Chambers (Dts), a drift cell has 42 mm width and 13 mm height as shown in Figure 3.12. Each cell is included up to 60 tubes between SLs. The 4 cm-wide tubes, containing a wire, is filled with a gas volume which contains mixture of Ar 85% and CO_2 15%. When a particle traverses into chamber and tube, it releases electrons by ionising this mixture of gases along its trace. Effect of the electric field between cathode and anode, the ionisation electrons drift with a typical velocity of some 10 μm/ns towards the anode wire. By beginning of drifting towards to anode, at the same time the fast signal from the tube starts a timer. The signal created at the anode as drifting electrons arrive then stops the timer to yield the drift time. The principle of drift tube chamber is based on measuring the drift time of the electrons coming from an ionising event in order to obtain spatial information. The drift time is the time elapsed since the moment of a particle transit, given by a trigger, and the signal measurement of the tube.

With a known drift velocity , the drift distance is obtained [41]. The maximum drift length is 2.0 cm and the single point resolution is 200 μm. Each station is designed to give a muon vector in space, with a (precision better than 100 μm in position and approximately 1 mrad in direction [35].

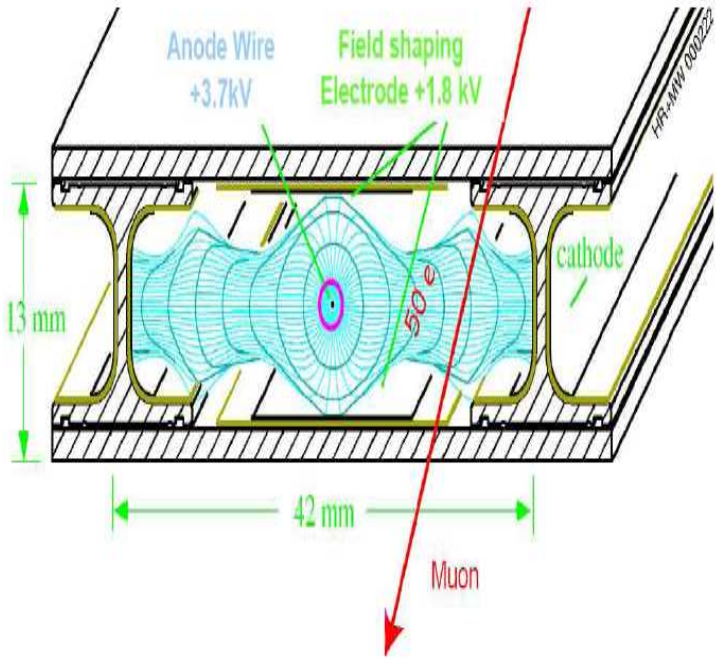

Figure 3.12: Cross section of drift cell with drift lines of electrons and isochrones.

- **Cathode Strip Chambers :** The Cathode Sitrip Chambers (CSCs) which are placed in each of 2 endcaps as 468 pieces, are housed in the Muon Endcap (ME) system. Both of CMS endcap regions consist of four discs (ME1 - ME4 from inside to outside) per endcap by fixing onto the endcap iron yokes as shown in figure 3.13. The innermost disc ME1 is divided into two concentric rings, ME2, ME3, ME4 are divided into three rings. There are 36 chambers in each ring of a muon station at the ME1 disc per endcap. The rings of other discs (ME2, ME3, ME4) are composed of 18 chambers [43]. The rings of discs are composed of trapezoidal multiwire proportional chambers. A single chamber consists of 6 equal layers of CSCs with segmented cathode read out.

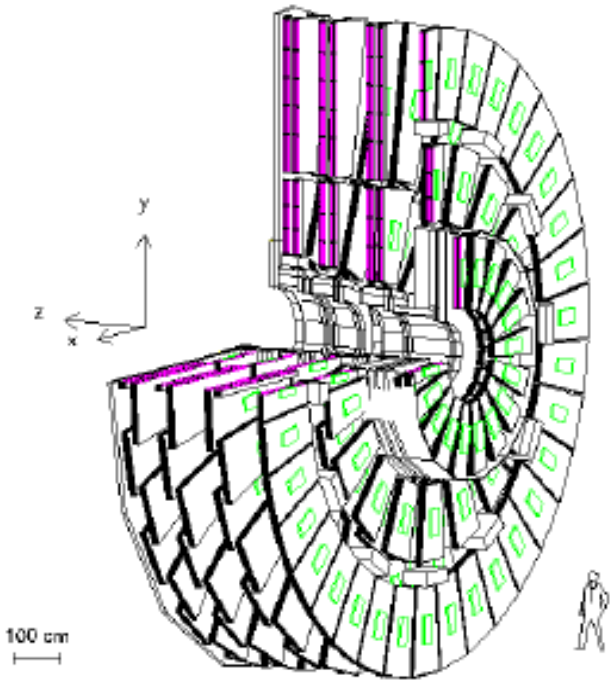

Figure 3.13: CMS Muon Endcap System.

Each layer is divided into two cathode planes which have a gas gap filled with $Ar(40\%), CO_2(50\%), CF_4(10\%)$ and an anode wire layer as single independent detector between the cathode planes. The cathode plane is divided into strips with a width between 3.5 mm and 16.0 mm. The anode wires in the cathode strips are placed perpendicularly within a pitch anode between 3 mm and 4.75 mm. By means of this perpendicular settlement, two positions of coordinate are obtained for each passing particle [37]. When a charged particle traverses each plane of a chamber, it produces a charge coming from free electrons by collecting on the anode wire and an image current on a group of cathode strips as shown in Figure 3.14. Penetrating particles ionise the chamber gas and causes an avalanche amplication within the applied electric field. A signal is obtained from moving charges on several strips of the cathode plane. In order to measure the position of a charged track the curvature of track in r, ϕ plane and rapidity η are used by anode wires. A precise position measurement is made by determining the centre-of-gravity of the charge distribution induced on the cathode strips [31].

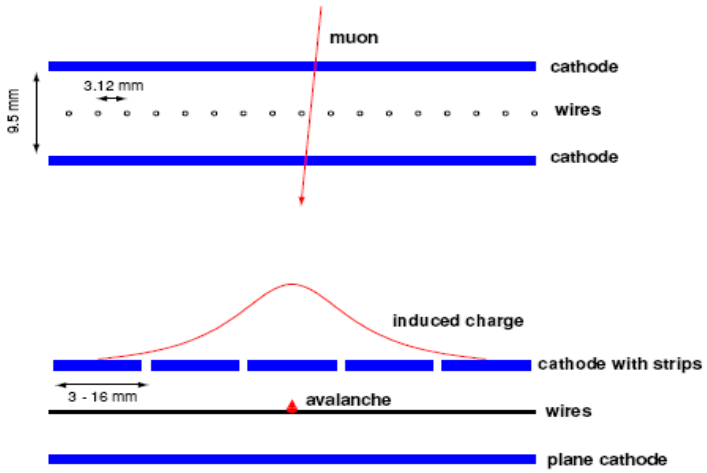

Figure 3.14: View across the wires (at the top) and across the cathode strips (at the bottom). Small spaces between the wires allow a fast chamber reaction whereas the track coordinate in wire direction can be measured via interpolation of the charge distribution.

Each CSC measures up to 6 space coordinates (r, ϕ , z). The spatial resolution provided by each chamber from the strips is typically about 200 μm (100 μm for ME1/1). The angular resolution in ϕ is of order 10 mrad [31].

- **Resistive Plate Chambers :** Resistive Plate Chambers (RPCs) are contained in both of barrel and endcap region of the muon system. The system comprises 4 stations covering the pseudorapidity region up to $|\eta|<$ 2.1 [23]. However, a shortfall of funds has led to the staging of the chambers sitting beyond $|\eta|>$ 1.6. RPCs in the first endcap station are also used to help resolve ambiguities in the CSCs [31]. There are 36 chambers mounted in each of 2 rings in each of the endcap stations. Each RPC detector consists of a double-gap bakelite chamber as shown in Figure 3.15, operating in avalanche mode [27]. RPCs consist of two high resistive parallel bakelite plates, a positively-charged anode and a negatively-charged cathode, both made of a very high resistivity plastic material and separated by a gas volume which is filled with a mixture of $C_2H_2F_4$ 96%, C_4H_{10} 3.5%, SF_6 0.5%. The outer surfaces of the resistive plates are coated with a thin graphite film as conductor forming high voltage and ground electrodes.

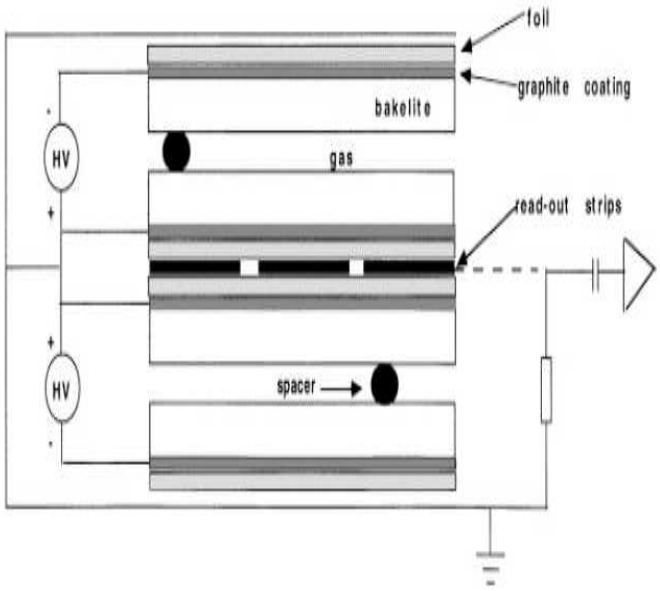

Figure 3.15: Schematic view of the RPC double-gap structure. The read-out strips in the Barrel chambers run along the beam direction.

A voltage of 9.5 kV is applied to the graphite coating, so that the field is strong enough to provide gas amplication in the gas gap. A traversing particle releases electrons from the gas inside a RPC which drift towards the anode, starting an avalanche as shown in Figure 3.16. When the avalanche reach the bakelite plates, they are discharged. Finally the bakelite plate is reached and penetrated slowly in the following until the electrons arrive at the graphite coating. An electric field is generated by two cathodes at the end plates and the anode wire in the middle of the cell. The E-field is formed by field shaping strips at the top and bottom side. Thus, a drift field of around 100V/mm to 250V/mm is generated. The created free electrons at the shortest distance (fastest distance) to the anode wire will reach it first. Near the anode drifting electrons cause an avalanche in the gas and a electrical signal is created.

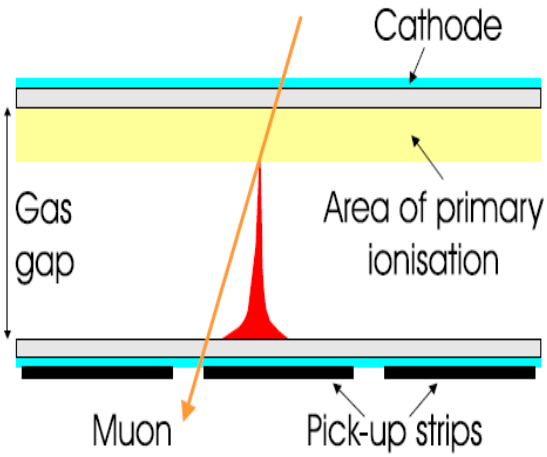

Figure 3.16: Operating mode of a resistive plate chamber in principle.

By measuring the time difference to an external trigger, e.g. by the RPCs, the distance of the track to the anode wire can be determined. By combination of many cells the track of a particle can be reconstructed. A measured point of a particle track in one cell is called hit. The time resolution basically depends on the drift distance in the gaseous material while the choice of the resistive plate parameters has a major influence on the compatibility with the expected particle rates. The construction and operation parameters for CMS RPCs yield a precision of muon (μ) in 3 ns [43].

The RPCs are used because of having a very fast signal response ($< 3ns$) and an excellent time resolution of $t < 1.3$ ns [44]. This is the reason that the RPCs are a good choice for space-time particle tracking as needed for the muon trigger.

CHAPTER 4

DATA PROCESSING

4.1 Data Organisation [45]

A physicist, who wants to see the data to extract a physics message for a high energy physics analysis, has to combine a variety of information:

- reconstructed information from the recorded detector data, specified by a combination of trigger paths and possibly further selected by cuts on reconstructed quantities (e.g., two jets),
- Monte Carlo samples which simulate the physics signal under investigation, and
- background samples (specified by the simulated physics process).

The datasets are split off at the Tier0 (T0) and distributed to the Tier1 (T1s), as described above. An event collection is the smallest unit within a dataset that a user can select. Typically, the reconstructed information needed for the analysis, as in the first bullet above, would all be contained in one or a few event collection(s). The expectation is that the majority of analyses should be able to be performed on a single primary dataset. Data are stored as ROOT files. The smallest unit in computing space is the file block which corresponds to a group of ROOT files likely to be accessed together. This requires a mapping from the physics abstraction (event collection) to the file location.

4.2 The CMS Data Hierarchy [45]

CMS Data is arranged into a hierarchy of data tiers. Each physics event is written into each data tier, where the tiers each contain different levels of information about the event. The different tiers each have different uses. The three main data tiers written in CMS are:

(1) **RAW** is full event information from the Tier0 (i.e. from CERN), containing 'raw' detector information (detector element hits, etc). RAW is not used directly for analysis.

(2) **RECOnstructed data (RECO)** is the output from firstpass processing by the Tier0. This layer contains reconstructed physics objects, but it still very detailed. RECO can be used for analysis, but is too big for frequent or heavy use.

(3) **Analysis Object Data (AOD)** is a "distilled" version of the RECO event information, and is expected to be used for most analyses. AOD provides a tradeoff between event size and complexity of the available information to optimise flexibility and speed for analyses.

It is the desire of CMS that the data tiers are written into separate files, though applications will be able to access more than one file simultaneously.

4.2.1 Data Flow Through Hardware Tiers

The flow of CMS detector data through the tiers is shown in the following Figure 4.1. The essential elements of the flow of real physics data through the hardware tiers are:

(1) T0 to T1 : Scheduled, timecritical, will be continuous during datataking periods. Reliable transfer is needed for fast access to new data, and to ensure that data is stored safely

(2) T1 to T1 : The Data is for redistributing data, generally after reprocessing (e.g. processing with improved algorithms).

(3) T1 to T2 : The Data is for analysis at Tier2s.

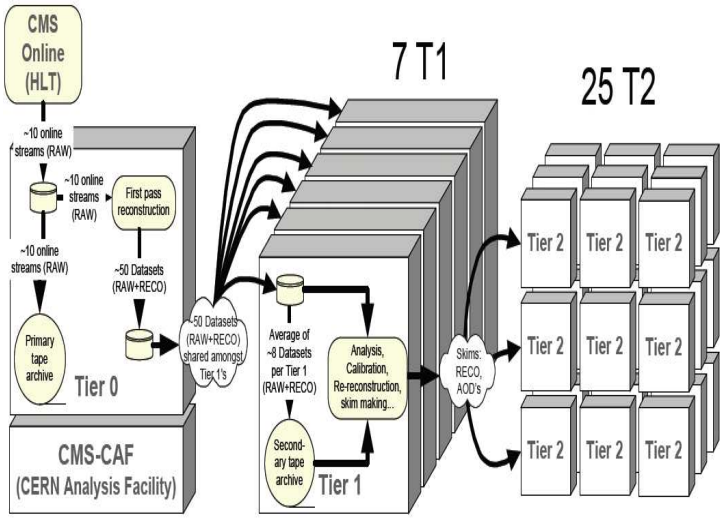

Figure 4.1: Detector Data Flow Through Hardware Tiers.

4.3 CMSSW [45]

The CMSSW framework implements a software bus model wherein there is one executable, called cmsRun, and many plugin modules which run algorithms. The same executable is used for both detector and MonteCarlo data. This framework is distinct from a more traditional approach in which several executables are used, one per task or set of tasks. The CMSSW executable, cmsRun, is configured at run time by the user's jobspecific configuration file. This file tells cmsRun which data to use, which modules to run, which parameter settings to use for each module, and in what order to run the modules. Required modules are dynamically loaded at the beginning of the job.

4.3.1 Event Data Model

The CMS Event Data Model (EDM) is centred around the concept of an Event as a C++ object container for all RAW and reconstructed data pertaining to a physics event. During processing, data are passed from one module to the next via the Event, and are accessed only through the Event. All objects in the Event may be individually or collectively stored in ROOT files, and are thus directly browsable in ROOT. This allows tests to be run on individual modules in isolation. Auxiliary information needed to process an Event is accessed via the EventSetup.

4.3.2 Modular Architecture

A module is a piece (or component) of CMSSW code that can be plugged into the CMSSW executable cmsRun. Each module encapsulates a unit of clearly defined eventprocessing functionality. Modules are implemented as plugins (core libraries and services). They are compiled in fullybound shared libraries and must be declared to the plugin manager in order to be registered to the framework. The framework takes care to load the plugin and instantiate the module when it is requested by the job configuration (sometimes called a "card file"). There is no need to build binary executables for user code.

When preparing an analysis job, modules are selected to run, and are specified a ParameterSet for each via a configuration file. The module is called for every event according to the path statement in the configuration file. There are six types of dynamically loadable processing modules, whose interface is specified by the framework:

(1) **Source** reads in an Event from a ROOT file or generates an Event for Monte Carlo, gives the Event status information (such as Event number), and can add data directly or set up a callback system to retrieve the data on the first request.

(2) **EDProducer** is used for the concept of producer modules and products, where producer modules (EDProducers) read in data from the Event in one format, produce something from the data, and output the product in a different format, into the Event by CMSSW.

(3) **EDFilter** reads data from the Event and returns a Boolean value that is used to determine if processing of that Event should continue for that path.

(4) **EDAnalyzer** reads data from the Event but is neither allowed to add data to the Event nor affect the execution of the path. Typically an EDAnalyzer writes output, e.g., to a ROOT Histogram.

(5) **EDLooper** can be used to control 'multipass' looping over an input source's data. It can also modify the EventSetup at well defined times.This type of module is used in the track based alignment procedure.

(6) **OutputModule** reads data from the Event, and once all paths have been executed, stores the output to external media. An example is PoolOutputModule which writes data to a standard CMS format ROOT file. The user configures the modules in the job configuration file using the modulespecific ParameterSets. ParameterSets may hold other ParameterSets. Modules cannot be reconfigured during the lifetime of the job. Once a job is submitted, the Framework takes care of instantiating the modules. Each bit of code described in the configuration file is dynamically loaded. The Data organisation scheme in CMSSW is shown in Figure 4.2. The process is as follows:

- First cmsRun reads in the config file and creates a string for each class that needs to be dynamically loaded.
- It passes this string to the plugin manager (the program used to manage the plugin functionality).
- The plugin manager consults the string-to-library mapping, and delivers to the framework the libraries that contain the requested C++ classes.
- The framework loads these libraries.
- The framework creates a parameter set (PSet) object from the contents of the (loaded) process block in the config file, and hands it to the constructor.
- The constructor constructs an instance of each module.
- The executable cmsRun, runs each module in the order specified in the config file.

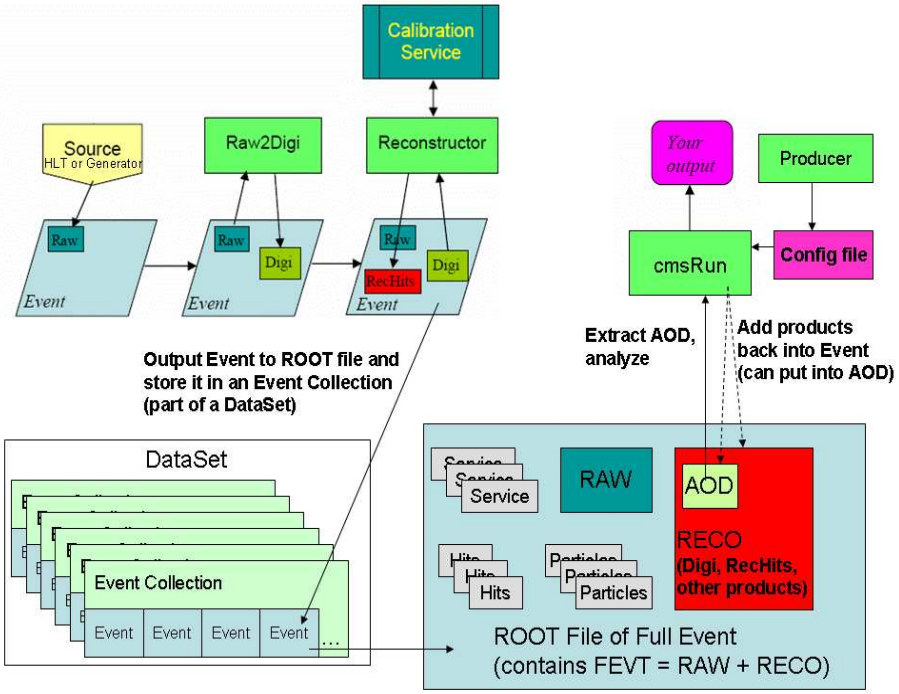

Figure 4.2: Data Organisation in CMSSW.

4.3.3 The Processing Model

Events are processed by passing the Event through a sequence of modules. The exact sequence of modules is specified by the user via a *path* statement in a configuration file. A path is an ordered list of *Producer*/*Filter*/*Analyser* modules which sets the exact execution order of all the modules. When an Event is passed to a module, that module can get data from the Event and put data back into the Event. When data is put into the Event, the provenance information about the module that created the data will be stored with the data in the Event as shown in Figure 4.3.

The Event is then passed to the execution paths. The paths can then be ordered into a list that makes up the schedule for the process. Since it will ask for exactly the same products from the event and produce the same result independent of which path it is in, it makes no sense to execute it twice. Each path should be executable by itself, in that modules within the path, only ask for things they know have been produced in a previous module in the same path or from the input source.

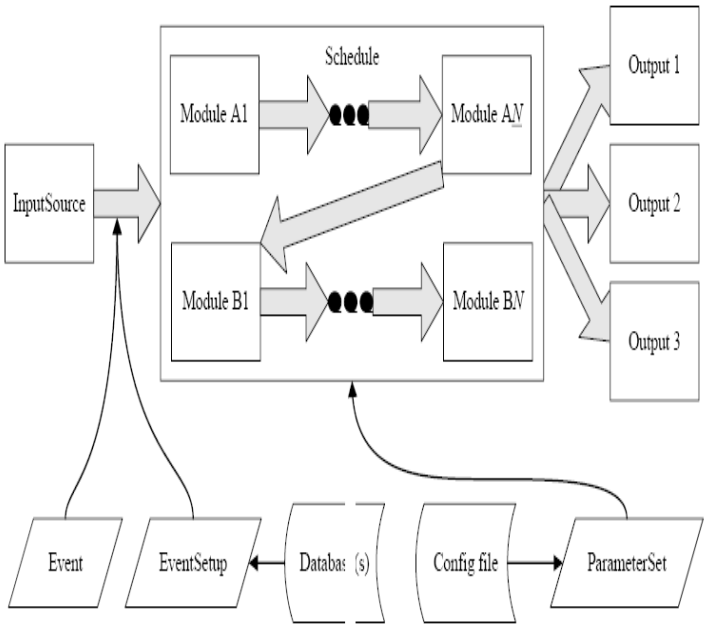

Figure 4.3: The components involved in the framework and EDM.

CHAPTER 5

LONG-LIVED EXOTIC PARTICLES

5.1 Nature of the Neutralinos

MSSM theory was explained in detailed in the second chapter. MSSM is an important theory because of the reason of between the electroweak gauginos and the higgsinos and within the various set of quarks and leptons and Higgs scalars sharing the same electric charge. The main production process for the SUSY Higgs boson h^0, the Feynman diagrams which are displayed in Figure 5.1, are the weak vector boson ($V = W\backslash Z$) fusion process $qq \rightarrow V^*V^* \rightarrow qq + h^0$, the associated Higgs production with heavy top or bottom quarks gg, $q\bar{q} \rightarrow q\bar{q} + h^0$, the gluon-gluon fusion mechanism gg $\rightarrow h^0$, the associated production with vector bosons $q\bar{q} \rightarrow h^0 + V$ and finally the quark antiquark fusion process $q\bar{q} \rightarrow h^0$ [46].

After electroweak symmetry breaking, the W^0, B^0, gauge eigenstates mix to give mass eigenstates Z^0 and γ, then transform their SUSY partners $(\tilde{B}, \tilde{W})$ and to give zino $(\tilde{Z}^0)$ and photino $(\tilde{\gamma})$. The charginos and neutralinos are the mass eigenstates of the $(\tilde{\mathrm{W}}^{\pm}, \tilde{H}^{\pm})$ and $(\tilde{\gamma}, \tilde{Z}, \tilde{H}^0)$ fields, respectively. The *neutralino* decays of higgs boson is shown in Figure 5.1. Several models including supersymmetry with R-parity violation [47, 48] and hidden valley theories [49] predict the existence of neutral, long-lived particles that give rise to a distinctive signature of two leptons arising from a highly displaced vertex. A generic term for new physics from a hidden sector new particles that can be relatively light hidden from the Standard Model by a barrier (for instance an energy barrier). High collision energies can produce particles in Hidden Valley.

Due to barrier these particles can be long-lived decay back into Standard Model particles e.g. in the Higgs sector [**?**].

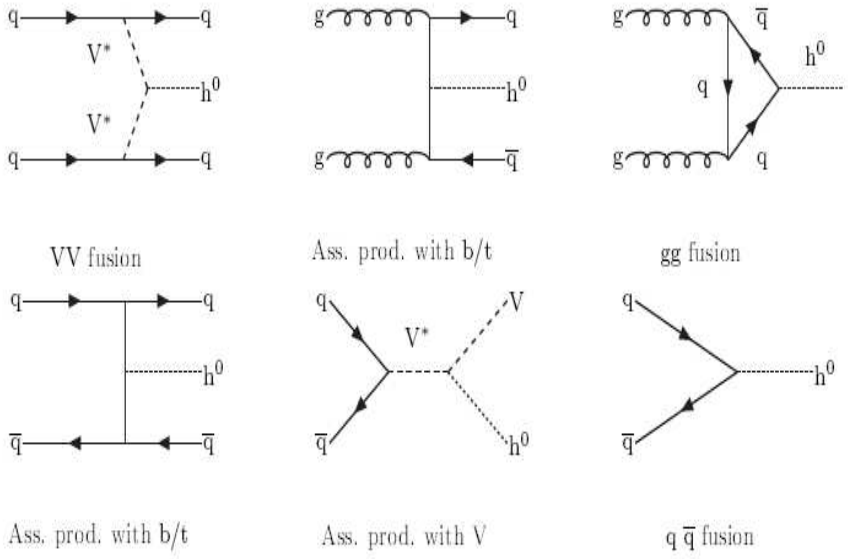

Figure 5.1: Dominant Feynman diagrams for Higgs production, listed by order of importance.

The Fermilab neutrino experiment NuTeV observed an excess of di-muon events that could be interpreted as such a signal [51, 52, 53]. Experiments at the CERN e+e Collider (LEP) have looked for short-lived neutralino and chargino decays [54] and long-lived charged particles [55], but did not search for this topology. In the LEP search, using e+e collision which decays to Z bosons, bb jets were searched with center of mass energies of 200 GeV and 400 GeV as shown in Figure 5.2. In these events, 1% of all bb events have two muons in the final state $\sim$ 10% with one events with muons originating apart from the impact parameter (IP). For comparison, number of displaced muons in the event and momentum of displaced the muons were shown in the Figure 5.2.

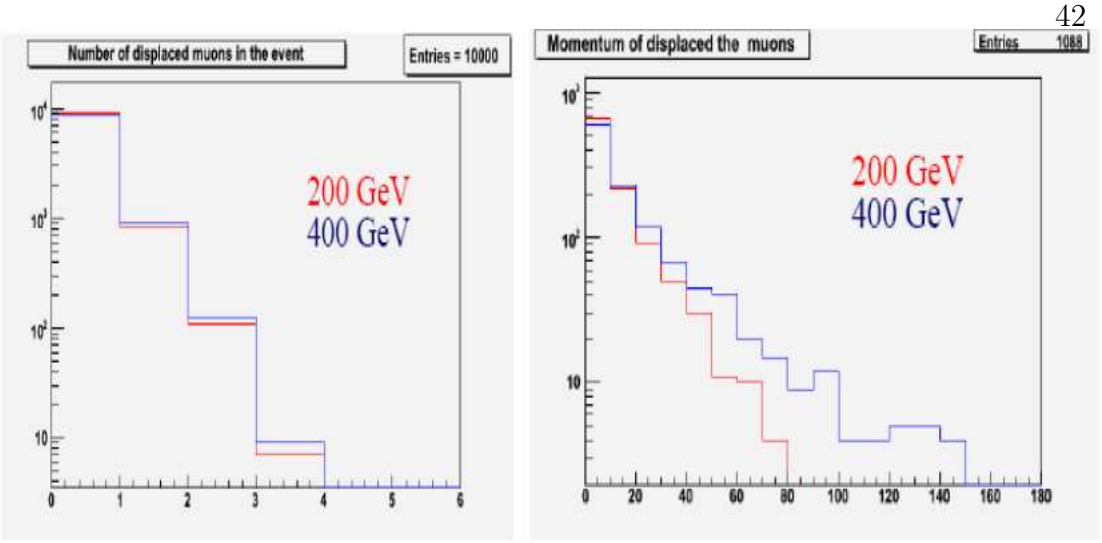

Figure 5.2: Left: Number of displaced muons in 10000 events. Right: Momentum of displaced the muons for these events.

As benchmark model, R-parity violating (RPV) decays of neutralinos (χ_1^0) to $\mu^+\mu^-\nu$ is used to determine signal efficiency as shown in Figure 5.3 [46]. Here the RPV couplings are expected to be small and lead to long lifetimes [56]. The results are applicable to any pair-produced neutral particle with similar kinematics. Also the feynman diagrams of neutralino pair production was illustrated in Figure 5.4.

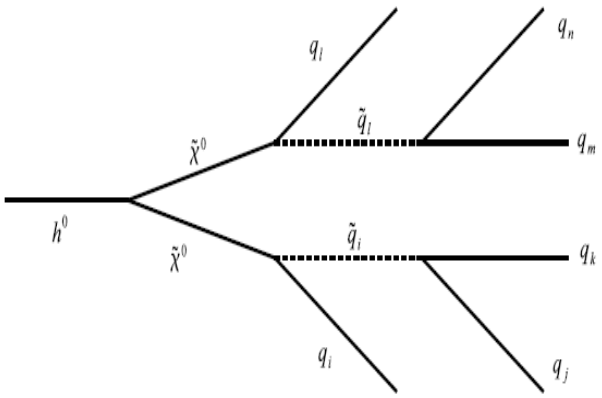

Figure 5.3: Diagram of the decay of Higgs to two neutralinos.

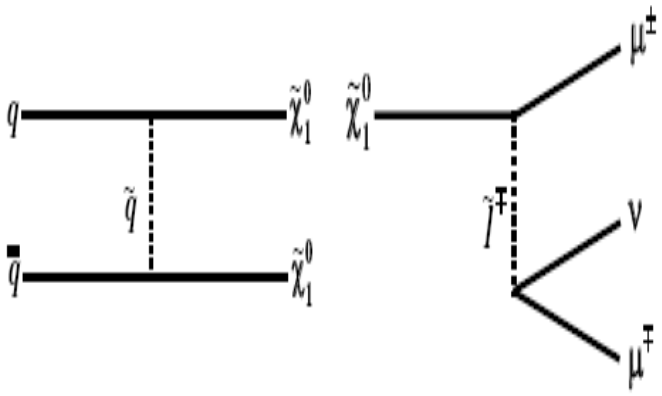

Figure 5.4: Feynman diagrams for pair production (left) and decay (right) of a neutral particle, in this case neutralinos with R-parity violation.

5.2 Event Generation

Monte Carlo Event Generators are used to generate high-energy-physics events, i.e. sets of outgoing particles produced in the interactions between two incoming particles. Generation is the first stage of the production of Monte Carlo event samples to be compared with real data, and to be used in background estimates. The generator creates a data event in memory for each iteration of the event loop in the configuration file, and puts the particles (or particle characteristics) it generates into the event. At LHC, Event generator position is shown in Figure 5.5. The following two steps are Simulation and Digitisation, whereby the newly generated particles are run through a simulation of the CMS detector, and the results are digitised to produce a final event which has the same format as a real data event observed in the CMS detector.

Several event generators are interfaced to CMSSW. They range from general-purpose ones (Pythia, Herwig, Sherpa) to more specific ones (Matrix Element calculators like Alpgen, MadGraph, generators for diffractive physics, cosmic muon generators, and so on). The objective of general-purpose event generators is to provide as accurate as possible a description of what happens in a particle collision. They contain theory and models for a number of physics aspects, such as hard and soft interactions, parton distributions, initial and final state parton showers, multiple interactions, fragmentation and decay.

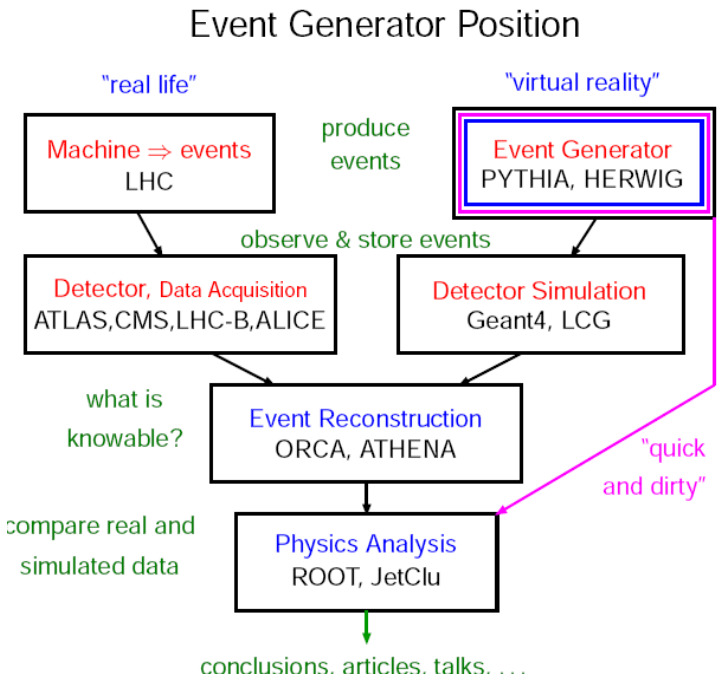

Figure 5.5: Event generator position at LHC.

5.2.1 Event Generation of The Neutralinos

New hidden valley or other long-lived particle models can be considered as tool boxes for possible new physics as shown in Figure 5.6. A Little Higgs model with T-parity violation was used for event generation. This model gives rise to heavy long-lived photons which can decay to jets or leptons.

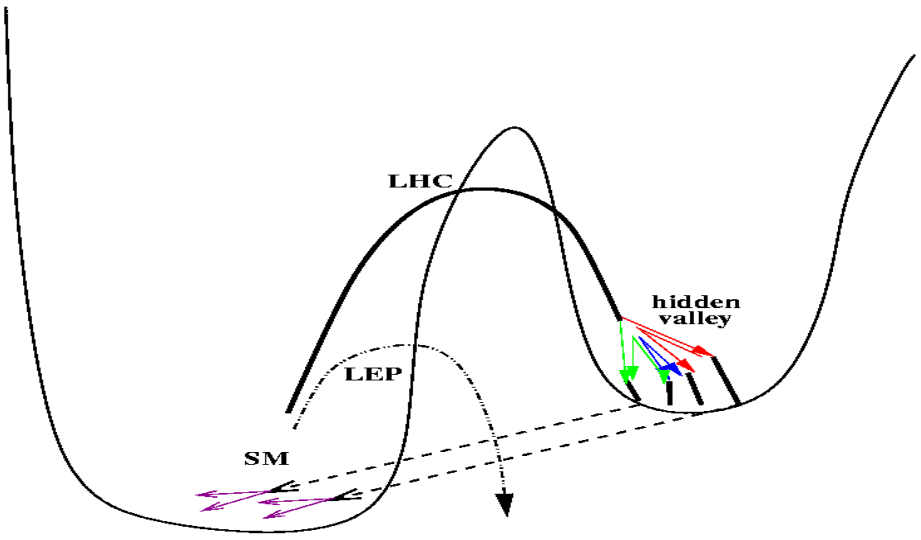

Figure 5.6: Diagram of the Hidden valley sector.

With the aid of the model:

- Heavy photons are produced by pairs in this model. So four partons are produced in the final state.
- Heavy photon mass and lifetime can be tuned.
- Partonic events generated with CalcHEP and then passed to Pythia for subsequent hadronization/decay/fragmentation.
- Then passed to standard CMSSW config files for simu/ digi/ reco/ trigger simu.

The full set of events used for this study has been generated with Pythia 6.4 as the main event generator used in CMSSW. In order to generate neutralino events in Pythia event generator, the supersymmetric particle codes were used in SUSY Les Houches Accord spectrum (SLHA). This is taken care of at initialisation if IMSS(1) parameter is positive. The complete neutralino configuration file which was used to generate the event, was attached into appendix section in Chapter 7. For event generation, firstly the transverse decay length was used as 30 mm for maximum two neutralinos decay.
In order to produce this event some SUSY Les Houches Accord spectrum (SLHA) parameters were used. For neutralino production, Particle ID '1000022' was initialised for 165 GeV neutralinos. In this event one of scenario, two jets decays was produced for each neutralino. This event was repeated 100 times according to Monte Carlo event generator method. The parameters which were used in configuration file of neutralino event generation is shown in Table 5.1.

Table 5.1: *Pythia Event Generation Codes for Neutralinos.*

IMMS(1)= 11	SUSY MSSM mass spectrum from a SLHA file
MSEL=0	Full user control
MSUB(...)=1	h^0 production subproccess
MSTP(41)=2	perform for all resonance decays,
IMSS(21)=82,IMSS(22)=82	jets in SLHA decay table
MSTJ(22)=2	average lifetime is smaller than PARJ(71)
PARJ(71)=10	average lifetime in mm
MWID(310)=0	Switch off some resonance particle

Due to their slow movement, yet high momentum, with weakly interacing properties, long-lived particles, posses very distinct features when they traverse ordinary matter. The typical signatures for the detection of these particles are :

- High transverse momentum for charged particle.
- Large ionisation in the tracking system, in case the particles are charge and slow.
- A characteristic pattern of energy deposition in the calorimeters.
- A large time-of-flight, measurable with especially in drift tubes in the muon chambers.

In order to compute time of flight information, DT wires are staggered. A muon (or any other charged particle reaching DTs) leave both left and right hits. Then hit position is measured by drift time, If t0 is not that of a $\beta = 1$ particle the hits are not aligned. So Realigning of the hits allow to compute the δT vs a $\beta = 1$ particle as shown in Figure 5.7.

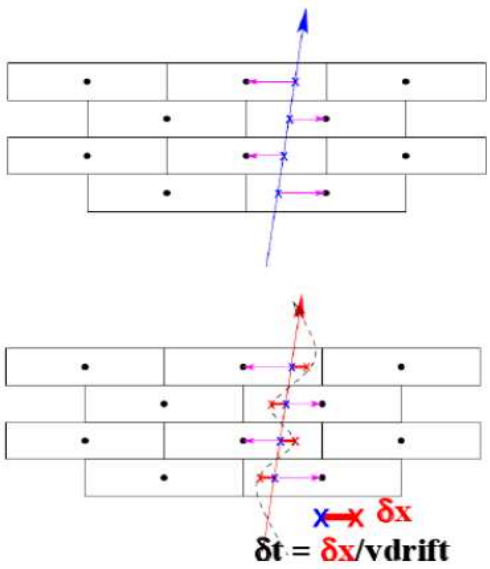

Figure 5.7: Time of Flight Information.

5.2.2 Simulation of Reconstructed Neutralinos

Signals in the outer part of muon system may not have tracker hits and should not rely on reconstruction including only tracker. Because of these both calorimeter for missing transverse energy and muon chamber for measuring the momentum is required for detection of the particle which is wanted to be found. Some parameter were used for calorimeter searches during the reconstruction.

DisplacedCaloJetProducer was newly developed to find vertex of origin for a jet (vertex farthest from calorimeter, containing at least 1 % of its energy) as shown in Figure 5.8 [57]. By rewriting new jet collection with vertex associated, Physical four-vector is recomputed with respect to vertex of origin on a per-jet basis. Samples for one particular hidden-valley model was generated for high p_t dijet signature missing E_t handle on jet originating inside the tracker volume. The tracks can be reconstructed and displaced to identify the decays.

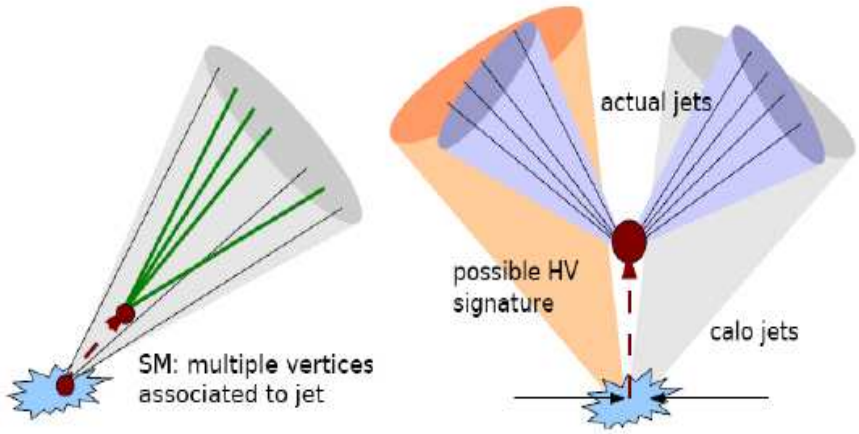

Figure 5.8: Possible Hidden-valley signatures in jets.

In these particular Hidden Valley events, the tracks mostly point towards the interaction point, they just start somewhere in the tracking system (in fact most of the vertices found are the actual origin of the hidden-valley jet) as shown in Figure 5.8 [57]. For generic dijet final state, there are two reconstruction ideas. The first idea is finding both vertices by giving all tracks in event to $MultiVertexFinder$. But this method will give poor performance. The second idea is reconstruct track jets Reconstruct χ^0 vertices by giving MultiVertexFinder only tracks in jets believed to have come from one χ^0. In order to obtain better performance the second idea was used by searching for reconstructed muons tracks as shown in Figure 5.9 [57].

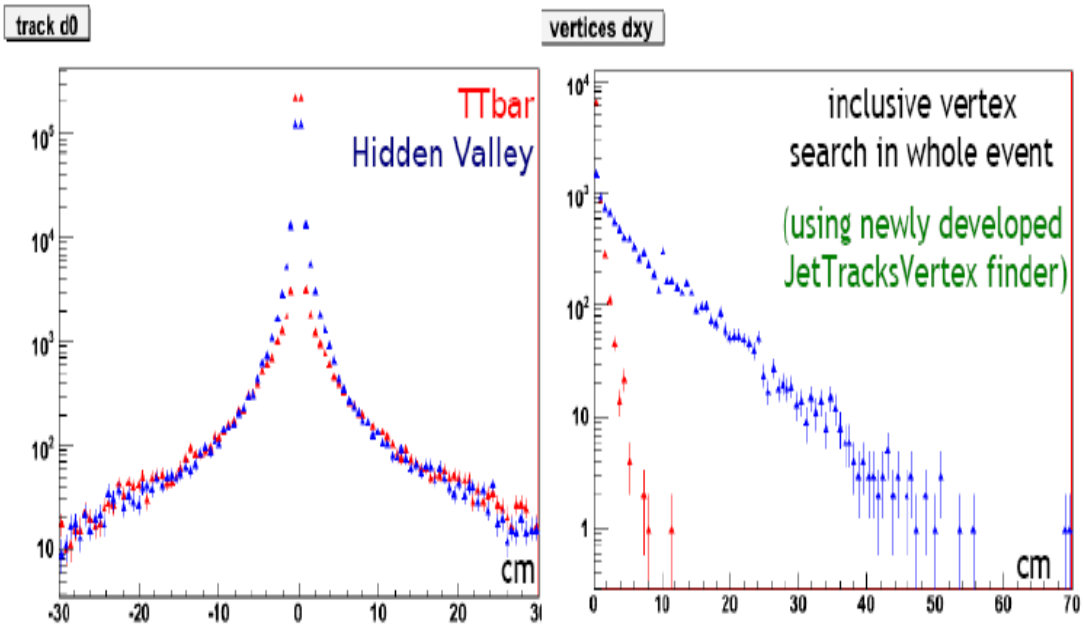

Figure 5.9: Reconstruction of neutralino vertices by using MultivertexFinder.

For simulation of this event, supposing that a massive, neutral, exotic particle of neutralinos was produced flies for 30 mm and then decays to b-jets. The simulation file which was used in CMSSW, was shown in appendix part at Chapter 7 too. The Calorimeter jets were used for missing transverse energy. CaloJets coming from χ^0 decay to have incorrect direction, since assume jet produced at primary vertex (P.V) as shown in Figure 5.10. The vertex is used to correct nearest CaloJet direction [58].

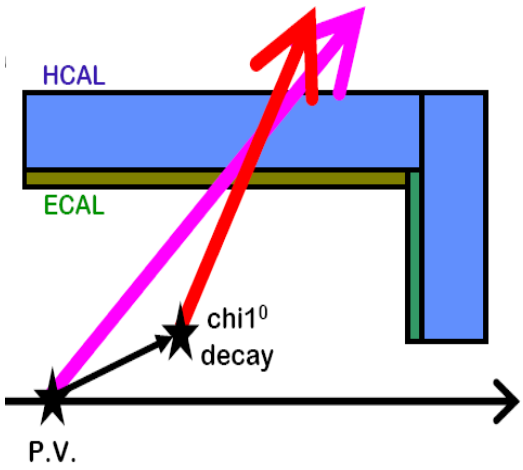

Figure 5.10: Calojet Correction.

This assumes the χ^0 decay vertex is known and includes an assumption about the depth in the calorimeters of the energy deposit. The primary vertex of neutralinos is shown in Figure 5.11.

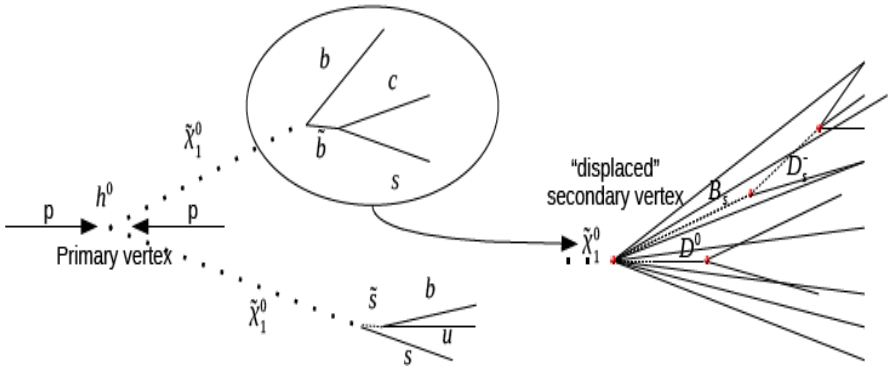

Figure 5.11: Primary vertex of neutralinos decay.

After generation of the event, the required steps, simulation and digitisation were performed by using CMSSW as python format. After all this file was converted to reconstruction format which is used for analysis as root file. This file was also converted to root file format to obtain the graphics below. The Figure 5.12 shows missing transversed energy in the Calorimeter.

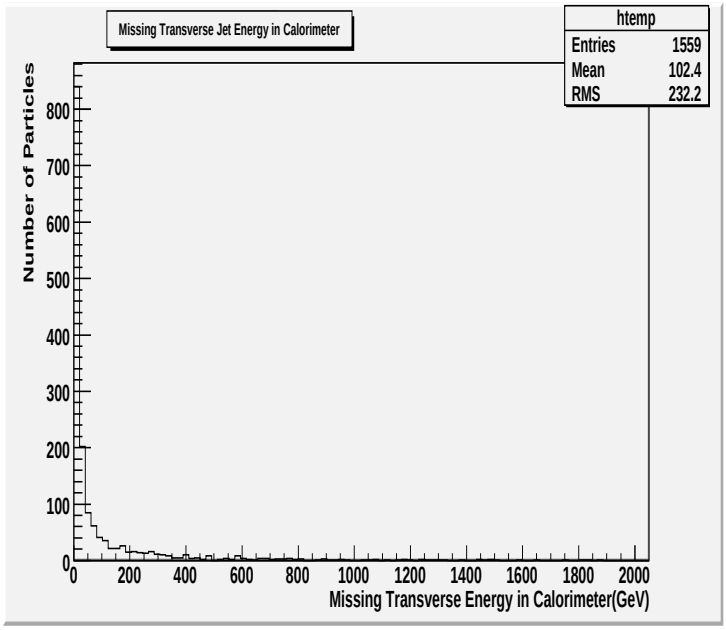

Figure 5.12: Missing Transverse Energy in the Calorimeter.

The last parameter of the searching neutralinos is vertex displacement. It was plotted in all-direction of muons. For x-direction, it was shown in below Figure 5.13.

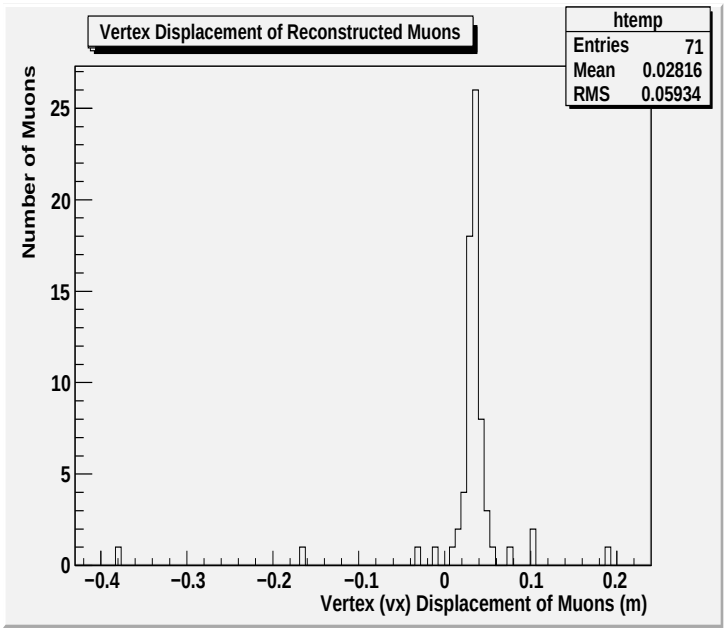

Figure 5.13: Vertex displacement in the x-direction of Reconstructed Muon.

Also other displacement parameters as y and z directions were shown for searching neutralinos in the vertex displacement as shown in Figures below.

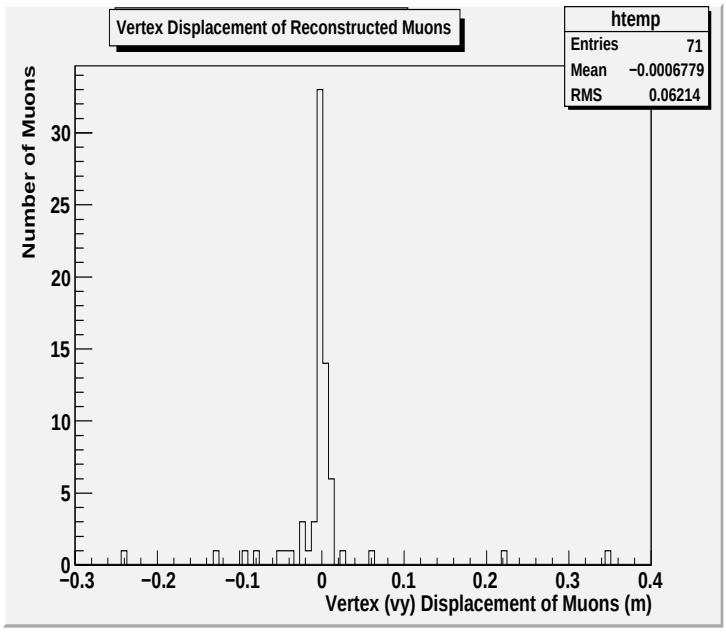

Figure 5.14: Vertex displacement in the y-direction of Reconstructed Muon.

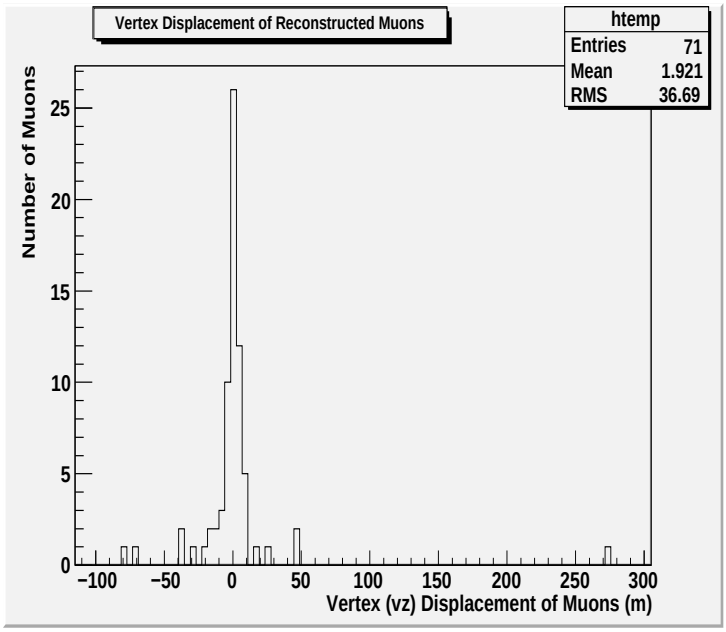

Figure 5.15: Vertex displacement in the z-direction of Reconstructed Muon.

CHAPTER 6

CONCLUSION

In this chapter, the arguments and results obtained in the present study were summarised for Supersymmetry searches with the CMS detector at LHC. If Supersymmetry is realised in Nature, sparticles will be easily produced at LHC. Especially if squarks and gluinos exist, they will be produced in abundance because of their strong interaction and will cascade to the lightest superpartrner in case of R-parity conservation. As it is neutral and weakly interacting, it will escape from the detection. Then missing energy, carried away by the LSP would be leading experimental signature of SUSY. It will be thereby possible to discover the superpartners up to a mass 2.5 TeV by variety of distinctive signature (multiple jets, multi-leptons, missing transverse energy) that are characteristic of minimal supersymmetric models. All kinematically accessable SUSY particles (charginos, neutralinos and sleptons) are produced simultaneously either directly or cascade decays of squarks and gluinos. So there will be many SUSY process.

One of them is about to R-parity. In R-parity conserving models the sparticles are expected to be produced in pairs, decaying sequentially until the lightest supersymmetric particle is reached. At the end, in addition to the neutrinos escaping detection there are two massive $\tilde{\chi}^0$'s also interacting weakly with ordinary matter. Thus, event signatures with a relatively large missing transverse energy are canonical for R-parity conserving models. In R-parity violating models the production of sparticles and their decays lead to signatures with no missing transverse energy thus drastically from the canonical signatures of R-parity conserving models.

In this study signatures of neutralinos decaying into jets were shown. After just 10 TeV center of mass energy of p-p collision, the 165 GeV mass of created neutralino is decayed into 2 jets. In order to identify neutralinos in the analysis two parameters will be basically used. Because of hardly interacting particle of neutralino, the missing transverse energy in Calorimeter is used for identification. Other parameter is reconstructed muons to find the tracks of the particle. In

100 events with 200 neutralinos, we have 71 muons. So this abundance is good reason for detection of neutralinos. Because of the structure of muon chamber which is placed into magnet system like a sandwich in CMS, Muons are good identification instrument. If this scenario is a true in nature, we are expected to find the neutralino and this kind of long-lived exotic particles in the first years of operating of CMS.

LIST OF REFERENCES

[1] A. Pich, *The Standard Model of Electroweak Interactions*, arXiv:hep-ph/9412274v1, (12 Dec 1994).

[2] M. Herrero, *The Standard Model*, arXiv:hep-ph/9812242v1, (3.12.1998).

[3] Kane G. L., *Modern Elemantary Particle Physics*, (1994).

[4] S. P. Martin, *A supersymmetreic primer appeared in: Perspectives on symmetry by G.Kane, Advenced Series on Directions in High Energy Physics,* **Vol. 18**

[5] A. C. Kraan, *Neutrinos: masses, mixing and decay, Thesis of Msc Degree (Agust 2001)*, www.nbi.dk/ ackraan

[6] L. Alvarez Gaumé, J. - P. Blaizot, M. Cvetič, M. Doser, D. F. Geeseman, G. F. Guidice, B. Grinstein, W. Haxton, V. Metag, A. Ringwald, L. Rolandi, W. -D. Schlatter, H. Weerts, T. Yanagida *Physics Letters B, Review of Particle Physics July 2008*, **Vol. 667, Issues (1-5)** 1212-1216, (18.09.2008).

[7] L. Girardello and M. Grisaru, *Nucl. Phys.* **B194**, 65 (1982).

[8] L. J. Hall and L. Randall, *Phys. Rev. Lett.* **65**, 2939 (1990); I. Jack and D. R. T. Jones, *Phys. Lett.* **B457**, 101 (1999).

[9] E. Witten, *Nucl. Phys.* **B188**, 513 (1981)

[10] S. Dimopoulos and H. Georgi, *Nucl. Phys.***B193**, 150 (1981).

[11] N. Polonsky, *Extensions of the standard model, Lect. Notes Phys.* **M68, 1** (2001).

[12] H. E. Haber and G. L. Kane, *Phys. Reports* **117**, 75 (1985).

[13] M. Drees, R. Godbole, and P. Roy,*Theory and Phenomenology of Sparticles, World Scientific, Singapore*, (2005).

[14] P. Fayet, *Phys. Lett.* **69B**, 489 (1977); G. Farrar and P. Fayet, *Phys. Lett.* **76B**, 575 (1978).

[15] G. Jungman, M. Kamionkowski, and K. Griest, *Phys.Reports* **267**, 195 (1996).

[16] A. R. Liddle and D.H. Lyth, *Phys. Reports* **213**, 1 (1993).

[17] P. Fayet, *Phys. Lett.* **84B**, 421 (1979); *Phys. Lett.* **86B**, 272 (1979).

[18] P. van Nieuwenhuizen, *Phys. Reports* **68**, 189 (1981).

[19] S. Deser and B. Zumino, *Phys. Rev. Lett.* **38**, 1433 (1977); E. Cremmer et al., *Phys. Lett.* **79B**, 231 (1978).

[20] Arkani-Hamed and S. Dimopoulos, *JHEP 0506*, 073 (2005); G.F. Giudice and A. Romanino, *Nucl. Phys.* **B699**, 65 (2004) [erratum: B706, 65 (2005)].

[21] N. Arkani-Hamed et al., *Nucl. Phys.* **B709**, 3 (2005); W. Kilian et al., *Eur. Phys. J.* **C39**, 229 (2005).

[22] K. Cheung and W. Y. Keung, *Phys. Rev.* **D71, 015015** (2005); P. Gambino, G.F. Giudice, and P. Slavich, *Nucl. Phys.* **B726**, 35 (2005).

[23] ATLAS Collaboration, *ATLAS Technical Proposal, CERN/LHCC 94-43* (1994).

[24] TOTEM Collaboration, *TOTEM Technical Design Report, CERN-LHCC-2004-002* (2004).

[25] CMS Collaboration, *CMS Physics Technical Design Report Volume II: Physics Performance, CERN/LHCC 2006-021* (2006).

[26] ATLAS Collaboration, *ATLAS Detector and Physics Performance Technical Design Report Volume II, CERN/LHCC 99-15* (1999).

[27] M. Abbrescia et al. 2006 5pp., *Production and quality control of the barrel RPC chambers of the CMS experiment.* Prepared for 9th Topical Seminar on Innovative Particle and Radiation Detectors (Siena 2004), Siena, Italy, (23-26 May 2004). *Nucl. Phys. Proc. Suppl.*, **150**, 290-294, (2006).

[28] M. Abbrescia et al. 2005. 11pp., *Cosmic ray tests of double-gap resistive plate chambers for the CMS experiment. Nucl. Instrum. Meth.* **A550**, 116-126, (2005).

[29] Genchev and Litov, *Study of the CMS TP Calorimetry system*, **CMS TN-1994/272**.

[30] The CMS colloboration, *The Magnet Project Techinal Design Report, CERN/LHCC 97-10*, (1997).

[31] The CMS Colloboration, *CMS Physics TDR Volume 1. CERN/LHCC 2006-001*, CMS TDR 8.1 (Feb 2006).

[32] The CMS colloboration, *The Level-1 Trigger -Technical Design Report Volume 1, CERN/LHCC 2000-038*, (December 2000).

[33] The CMS pixel detector, http://cms.web.psi.ch/cms.html

[34] L. Borrello, A. Messineo, E. Focardi, and A. Macchiolo, *Sensor design for the CMS Silicon Strip Tracker, CMS Note 2003-020* (2002).

[35] CMS Collaboration, *Addendum to the CMS Tracker Technical Design Report, CERN/LHCC 2000-016*, February (2000).

[36] CMS Collaboration, *The Tracker System Project - Technical Design Report, CERN/LHCC 94-38*, December (1994).

[37] The CMS Experiment Official Website, http://cmsinfo.cern.ch

[38] CMS Collaboration, *The Electromagnetic Calorimeter Project - Technical Design Report, CERN/LHCC 97-33*, December (1997).

[39] CMS HCAL, *Design, Performance, and Calibration of CMS Hadron-Barrel Calorimeter Wedges*, *Nucl. Instrum. and Methods*, (2005).

[40] CMS HCAL, *Design, Performance, and Calibration of CMS Hadron-Endcap Calorimeter Wedges*, *Nucl. Instrum. and Methods*, (2005).

[41] Leo W. R., *Techniques of Nuclear and Particle Physics Experiments*, Springer (1987).

[42] CMS Collaboration, *The Compact Muon Solenoid, Technical Proposal, CERN/LHCC 94-38*, (1994).

[43] CMS Collaboration, *The Muon Project, Technical Design Report, CERN/LHCC 97-32*, (1997).

[44] S. H. Ahn et al; *Nucl. Instr. and Meth.*, **A469**, 323, (2001).

[45] The CMSSW Documentation Suite, https://twiki.cern.ch/twiki/bin/view/CMS/WorkBook

[46] Neal Gueissaz, *Searching For a Supersymmetric Higgs Boson through displaced Decay Vertices in LHCB.*, (2007).

[47] S. P. Martin; *arXiv:hep-ph/9709356.*

[48] R. Barbier et al.; *Phys. Rept.*, **420**, (2005).

[49] M. J. Strassler and K. M. Zurek; *arXiv:hep-ph/0604261, arXiv:hep-ph/0605193.*

[50] Christophe Saout et al.; *Displaced Jets in Hidden Valley Events*, Exotica Meeting, CERN, (21.10.2008).

[51] T. Adams et al. [NuTeV Collaboration]; *Phys. Rev. Lett.* **87,041801.**, (2001).

[52] L. Borissov, J. M. Conrad, and M. Shaevitz; *arXiv:hep-ph/0007195.*

[53] A. Dedes, H. K. Dreiner, and P. Richardson; *Phys. Rev.D 65, 015001.*, (2002).

[54] J. Abdallah et al. [DELPHI Collaboration], *Eur. Phys. J.C* **36**, 1 (2004), erratum *Eur. Phys. J.* **C 37**, 129 (2004); G. Abblendi et al. [OPAL Collaboration], *Eur. Phys. J.* **C 33**, 149 (2004); A. Heister et al. [ALEPH Collaboration], *Eur. Phys. J. C* **31**, 1 (2003); P. Achard et al. [L3 Collaboration], *Phys. Lett. B* **524**, 65 (2002).

[55] G. Abbiendi et al. [OPAL Collaboration], *Phys. Lett.B* **572**, 8 (2003); J. Abdallah et al. [DELPHI Collaboration], *Eur. Phys. J.* **C 27**, 153 (2003); A. Heister et al.[ALEPH Collaboration], *Eur. Phys. J.* **C 25**, 339 (2002); P. Achard et al. [L3 Collaboration], *Phys. Lett. B* **517**, 75 (2001).

[56] R. Barbier et al.; *arXiv:hep-ph/9810232.*

[57] Christophe Saout, *Search for Hidden-valley Decays in the Tracker Volume*, Hidden-Valley and Long-Lived Particles Workshop, (14.01.2009).

[58] Ian Tomalin, *Reconstruction of Long-Lived Exotic Decays*, Exotica Meeting, CERN, (29.05.2008).

APPENDIX A

A.1 Generation of The Neutralino Events [1]

```
import FWCore.ParameterSet.Config as cms
from SimGeneral.HepPDTESSource.pythiapdt_cfi import
from Configuration.Generator.PythiaUESettings_cfi import

source = cms.Source("PythiaSource",
# Set my specific neutralino decay mods in PythiaSource.cc
decay_neutralinos = cms.untracked.bool(True),
max_neutralinos_decay = cms.untracked.int32(2),
# The following only work if PARJ(71) ¡ ctau of neutralino.
fixed_neutralino_trans_decay_length = cms.untracked.bool(False),
# if fixed, then transverse decay length in mm is ...
neutralino_trans_decay_length = cms.untracked.double(30.0),
neutralino_scale_lifetime = cms.untracked.double(1.5),

# Print event
pythiaPylistVerbosity = cms.untracked.int32(3),
# Print decay tables
pythiaHepMCVerbosity = cms.untracked.bool(True),
maxEventsToPrint = cms.untracked.int32(100),

# 10 TeV centre of mass energy.
comEnergy = cms.untracked.double(10000.),
```

[1] Some modules and parameters of the configuration and reconstruction files were used with permission of Ian Tomalin who is the member of Long-lived particles and Hidden-valley search group. The results were discussed in Sofia group of Long-lived particles and Hidden-Valley group.

```
        # possibility to run single or double back-to-back particles with PYTHIA
# if ParticleID = 0, run PYTHIA
DoubleParticle = cms.untracked.bool(True),

        # chi0_1
ParticleID = cms.untracked.int32(1000022),

        Ptmin = cms.untracked.double(250.),
Ptmax = cms.untracked.double(251.),
Etamin = cms.untracked.double(0.0),
Etamax = cms.untracked.double(2.0),
Phimin = cms.untracked.double(0.0),
Phimax = cms.untracked.double(360.0),

        PythiaParameters = cms.PSet( pythiaUESettingsBlock,
pythiaMyDecays = cms.vstring(
'MSTJ(22)=2  Decay those unstable particles',
'PARJ(71)=10.  for which ctau ¡ 10 mm',
# MSSM from SLHA file on unit 42 (chi0 → e + e−)or62(chi0 → mu + mu−)
#or82(chi0 → 2jet)
#Mass165GeV.

        'IMSS(1)=11',
'IMSS(21)=82',
'IMSS(22)=82',
'MSTP(41)=2  allow some resonance decays',
'MWID(310)=0  treat chi0 as ordinary particle',

        # Request neutralino pair production
'MSEL=0',
'MSUB(216)=1'),
parameterSets = cms.vstring('pythiaUESettings','pythiaMyDecays')))
```

A.2 Simulation of The Event

```
        import FWCore.ParameterSet.Config as cms

        process = cms.Process("Sim")
```

```
useParticleGun = False
print "Using particle gun  ", use ParticleGun

        process.maxEvents = cms.untracked.PSet( input = cms.untracked.int32(100))

        process.load("Configuration.StandardSequences.Services_cff")
process.load('Configuration/StandardSequences/FrontierConditions_GlobalTag_cff')
process.load('Configuration/StandardSequences/GeometryPilot2_cff')
process.load('Configuration/StandardSequences/MagneticField_38T_cff')
process.GlobalTag.globaltag = 'IDEAL_V9::All'
print "Using IDEAL_V9"

        process.load("FWCore.MessageService.MessageLogger_cfi")
process.MessageLogger.cout = cms.untracked.PSet( threshold = cms.untracked.string(
'WARNING'),INFO = cms.untracked.PSet( limit = cms.untracked.int32(100)
) )
        process.Timing = cms.Service("Timing")
process.options = cms.untracked.PSet(
wantSummary = cms.untracked.bool(True),
makeTriggerResults = cms.untracked.bool(True),
Rethrow = cms.untracked.vstring('Unknown',
'ProductNotFound',
'DictionaryNotFound',
'InsertFailure',
'Configuration',
'LogicError',
'UnimplementedFeature',
'InvalidReference',
'NullPointerError',
'NoProductSpecified',
'EventTimeout',
'EventCorruption',
'ModuleFailure',
'ScheduleExecutionFailure',
'EventProcessorFailure',
'FileInPathError',
'FatalRootError',
'NotFound') )
```

```
# Generate Pythia events. (Edit this file to change decay mode).
process.load("Configuration.Examples.Neutralinos_cff")
process.load("Configuration.StandardSequences.Generator_cff")
process.load("Configuration.StandardSequences.Sim_cff")
process.load("Configuration.StandardSequences.Digi_cff")
process.load("Configuration.StandardSequences.MixingNoPileUp_cff")
process.load("Configuration.StandardSequences.DigiToRaw_cff")
process.load("Configuration.StandardSequences.SimL1Emulator_cff")
process.load(
'L1TriggerConfig.L1GtConfigProducers.Luminosity.⇒
lumi1030.L1Menu2008_2E30_Unprescaled_cff')
process.load('HLTrigger.Configuration.HLT_2E30_cff')
process.load('HLTrigger.Configuration.HLT_2E30_cff')

# Beam spot - use this for particle gun, since easier if no beam-spot smear-
ing.
if useParticleGun:
process.load("Configuration.StandardSequences.VtxSmearedGauss_cff")
process.GaussVtxSmearingParameters.MeanX = 1.8
process.GaussVtxSmearingParameters.MeanX = 0.0
process.GaussVtxSmearingParameters.MeanY = 0.0
process.GaussVtxSmearingParameters.MeanZ = 0.0
process.GaussVtxSmearingParameters.SigmaX = 0.001
process.GaussVtxSmearingParameters.SigmaY = 0.001
process.GaussVtxSmearingParameters.SigmaZ = 0.001

# For particle gun, ensure reconstructed beam spot at 0,0,0
# process.BeamSpotFakeConditions.BeamType = 'SimpleGaussian'
print "Using zero-width Beam spot centred at 0"
else:
# or this for normal Pythia
process.load('Configuration/StandardSequences/VtxSmearedEarly10TeVCollision_cff')
print "Beam spot corresponding to early conditions"
# Define event content
process.load("Configuration.EventContent.EventContent_cff")
process.RECO = cms.OutputModule("PoolOutputModule",
process.FEVTDEBUGEventContent,
dataset = cms.untracked.PSet(dataTier = cms.untracked.string('GEN-SIM-RAW')),
fileName = cms.untracked.string('sim.root'))
```

```
    # Write events to disk
process.outpath = cms.EndPath(process.RECO)
    # Run everything
process.p0 = cms.Path(process.pgen
process.psim
process.pdigi
process.SimL1Emulator
process.DigiToRaw )
process.schedule = cms.Schedule(process.p0)
process.schedule.extend(process.HLTSchedule)
process.schedule.append(process.outpath)
```